A toolbox of engineered mosquito lines to study salivary gland biology and malaria transmission

Dennis Klug[1,#], Katharina Arnold[1], Raquel Mela-Lopez[1], Eric Marois[1] and Stéphanie A. Blandin[1]

[1]Université de Strasbourg, CNRS UPR9022, INSERM U1257, Institut de Biologie Moléculaire et Cellulaire, 67000 Strasbourg, France

to whom correspondence should be addressed:
dklug@unistra.fr

Keywords: malaria, sporozoite, *Anopheles gambiae*, aapp, trio, saglin, yellow, *in vivo* microscopy

Abstract

Mosquito saliva is a vehicle for the transmission of vector borne pathogens such as *Plasmodium* parasites and different arboviruses. Despite the key role of the salivary glands in the process of disease transmission, knowledge of host-pathogen interactions taking place within this organ is very limited. To improve the experimental tractability of the salivary glands, we have generated fluorescent reporter lines in the African malaria mosquito *Anopheles coluzzii* using the salivary gland-specific promoters of the anopheline antiplatelet protein (AAPP), the triple functional domain protein (TRIO) and saglin (SAG). Promoter activity was specifically observed in the distal-lateral lobes or in the median lobe of the salivary gland. Besides a comparison of the expression patterns of the selected promoters, the fluorescent probes allowed us to evaluate the inducibility of the selected promoters upon blood feeding and to measure intracellular redox changes. We also combined the *aapp-DsRed* fluorescent reporter line with a pigmentation-deficient *yellow(-)* mosquito mutant to assess the feasibility of *in vivo* microscopy of parasitized salivary glands. This combination allowed locating the salivary gland through the cuticle and imaging of individual sporozoites *in vivo*, which facilitates live imaging studies of salivary gland colonization by *Plasmodium* sporozoites.

Introduction

Vector borne diseases have been a major health burden in the history of mankind. An efficient way to counteract diseases transmitted by blood sucking arthropods is to prevent transmission by reducing the number of vectors in the environment or by preventing vectors from biting humans in risk areas. As a consequence of malaria control interventions, approximately 663 million clinical malaria cases could be averted between 2000 and 2015. The most effective measure was the use of insecticide treated bet nets, which prevented an estimated 68% of cases (Bhatt *et al.*, 2015). Still, preventive measures are counteracted by the very effective transmission of vector borne pathogens, which hampers eradication approaches. The key organ for transmission of vector-borne diseases is the salivary gland, as pathogens must colonize this organ to subsequently enter the saliva and be deposited in the skin during a blood meal. Host-pathogen interactions that take place in this organ are crucial for the spread of pathogens, as the concentration of pathogens in the mosquito saliva, as well as the composition and quantity of the saliva itself, are critical for successful transmission. To successfully colonize salivary glands, different pathogens have developed different strategies. While vector-borne viruses such as DENV cause systemic infection of the mosquito and replicate in the salivary glands (Salazar *et al.*, 2007), malaria parasites of the genus *Plasmodium* proliferate exclusively in the mosquito midgut. After infection of the mosquito midgut through the uptake of a blood meal from an infected host, *Plasmodium* parasites form a cyst, called oocyst, below the basal lamina of the midgut epithelium where they undergo multiple rounds of DNA replication. Rapid cell division, called sporogony, then follows, leading to the generation of several thousand of sporozoites per oocyst. These cells are released from oocysts and travel from the midgut to the salivary glands that they specifically recognize and invade. After being deposited along with mosquito saliva in the skin during a blood meal, sporozoites traverse the dermis, enter blood capillaries and reach the human liver where they pursue development. On the path of the sporozoite from the mosquito midgut to the liver of its intermediate host, the salivary glands represent a special niche in which the sporozoites mature before being transferred to the host with the mosquito saliva.

Although the general life cycle of *Plasmodium* is well known, we lack detailed knowledge of the temporal relationships and host-parasite interactions that occur in the various tissues and cells which the parasite, particularly the sporozoite, traverses and invades. While it is believed that the invasion process of the salivary glands by sporozoites that have egressed from oocysts is rapid (~1-10 minutes), *in vivo* data supporting this assumption is lacking (Douglas

98 *et al.*, 2015). Still, the time a sporozoite needs to reach and successfully invade the glands is
99 an important parameter, because at this timepoint, a mosquito is considered infective to
100 humans. In addition, microscopic examinations of infected glands revealed that sporozoites
101 form large aggregations in organized "stacks" in the cavities of the acinar cells. The degree of
102 order in these structures raises the question of whether the sporozoites recognize each other
103 and possibly enter a quiescent phase to bridge the time until the vector next blood meal, or
104 whether these stacks form by mechanical constraints alone. Based on the accumulation of
105 sporozoites in specific sub-regions of salivary glands, it has also been hypothesized that
106 sporozoites may preferentially invade the gland at specific sites (Wells and Andrew, 2019).
107 However, since no receptor-ligand interaction between sporozoites and acinar cells has yet
108 been clearly identified, the detection of such entry sites is difficult to prove. The study of
109 gland-sporozoite or sporozoite-sporozoite interactions in the gland has generally been limited
110 to the observation of infected tissues *ex vivo* because the highly pigmented cuticle of the
111 mosquito makes microscopy of parasite stages in living mosquitoes difficult and, at the same
112 time, an *in vitro* culture system for the insect stages of *Plasmodium* is not available. While *ex*
113 *vivo* studies significantly contributed to the knowledge about *Plasmodium* we have today,
114 samples obtained in this way are less suitable for imaging dynamic processes because
115 dissected tissues change and decompose rapidly. In addition the study of processes taking
116 place in salivary glands has been complicated by the lack of molecular tools for mosquitoes
117 like fluorescent reporter lines with tissue-specific gene expression, which have been slow to
118 develop due to difficulties in transgenesis. The implementation of CRISPR/Cas9 technology
119 in mosquito research has been a decisive step forward, which will give access to the analysis
120 of the molecular mechanisms underlying mosquito-pathogen interactions at an unprecedented
121 level of details. Females of *Aedes spp.* and *Anopheles spp.* mosquitoes possess two salivary
122 glands each consisting of two lateral lobes and one median lobe. In addition, the lateral lobes
123 are further subdivided into a distal-lateral and a proximal-lateral part which differ visually in
124 cell size and in the size of formed cavities in which cells secrete saliva components (Wells,
125 Villamor and Andrew, 2017). Transcriptomic studies have shown that salivary glands display
126 a tissue-specific expression profile in which many proteins thought to have a function in
127 blood uptake are indeed absent in male salivary glands (Arcà *et al.*, 2005). Consistent with the
128 reduction in expressed proteins, male salivary glands are smaller and differ in their
129 morphology, consisting of only one lobe per gland. Detailed knowledge about the expression
130 of proteins in the salivary glands could be obtained by applying *ex vivo* approaches. *In situ*
131 hybridization of gland-specific transcripts on dissected *Aedes aegypti* salivary glands has

132 shown that genes are spatially expressed in the median, distal-lateral, and proximal-lateral
133 lobes or combinations thereof (Juhn *et al.*, 2011) suggesting that different sections of the
134 salivary gland may provide different components of mosquito saliva. In addition, *Plasmodium*
135 sporozoites have been shown to invade primarily the distal-lateral lobes (Wells and Andrew,
136 2019), which has led to speculation about a specific protein interface used by sporozoites to
137 recognize the distal-lateral sections.
138 Recombinant salivary proteins considered to have therapeutic potential have been produced
139 and studied *in vitro* for their vasodilator, anticoagulant and anti-inflammatory properties.
140 Examples include aegyptin (Calvo *et al.*, 2010), anopheline (Figueiredo *et al.*, 2012), and
141 anopheline anti-platelet protein (AAPP) (Hayashi *et al.*, 2012), all of which act as
142 anticoagulants. From this selection, AAPP is one of the few proteins that have also been
143 studied *in vivo*. In *A. stephensi*, the generation of one of the first transgenic mosquito lines
144 showed that the *aapp* promoter drives DsRed expression exclusively in the distal-lateral lobes
145 (Yoshida and Watanabe, 2006). In addition to their primary physiological function, salivary
146 gland proteins suspected to play a role in the spread of pathogens such as the malaria parasite
147 *Plasmodium* have been the focus of several studies. Protein-protein interaction-based
148 approaches using sporozoite surface proteins and salivary gland proteins identified the
149 proteins saglin and CSPBP as potential determinants for sporozoite invasion (Ghosh *et al.*,
150 2009; Wang *et al.*, 2013). Knockdown experiments of both proteins have shown that
151 sporozoite numbers in the salivary glands are reduced compared to controls, indicating a
152 lower invasion rate. However, overexpression of saglin in the distal-lateral lobes of *A.*
153 *stephensi* did not result in an increase in the number of sporozoites colonizing the salivary
154 glands, raising doubt about the importance of saglin in this process (O'Brochta *et al.*, 2019).
155 Another protein that has been shown to affect sporozoite transmission is AgTRIO (triple
156 functional domain protein), that, like saglin, belongs to the SG1-protein family (Francischetti
157 *et al.*, 2002; Arcà *et al.*, 2005). Active and passive immunization of mice with recombinant
158 AgTRIO was shown to diminish transmission of *P. berghei* sporozoites (Dragovic *et al.*,
159 2018; Chuang *et al.*, 2019). Interestingly, TRIO expression increases in the presence of *P.*
160 *berghei* sporozoites, suggesting that sporozoites in salivary glands may influence protein
161 expression of their host cells to potentially increase transmission efficiency. (Dragovic *et al.*,
162 2018). Here we generated and characterised three fluorescent salivary gland reporter lines
163 using the upstream regions of the *aapp*, *trio* and *saglin* genes in the African malaria vector
164 *Anopheles coluzzii*, and we use one of them in combination with a pigment-deficient line to

perform *in vivo* live imaging of sporozoites invading salivary glands. We expect the lines described here will be of use to investigate salivary gland and sporozoite biology.

168 # Results

169

170 **Generation of transgenic mosquito lines with salivary gland-specific reporter expression**
171 **and low pigmentation**

172 To generate salivary gland reporter lines, the 5' upstream sequences of *saglin* (AGAP000610),
173 *aapp* (AGAP009974) and *trio* (AGAP001374) were used to drive the expression of DsRed
174 and hGrx1-roGFP2 from transgenic constructs integrated in the X1 docking line (**Fig. 1A, Fig.**
175 **1 – figure supplement 1A**) with an attP site on chromosome 2L (Volohonsky *et al.*, 2015).
176 The fluorescence reporter hGrx1-roGFP2 was chosen because it bears the advantages of
177 EGFP and enables the measurement of the oxidation level of the intracellular glutathione pool
178 by ratiometric quantification (Gutscher *et al.*, 2008). We used the *aapp* promoter sequence
179 from *Anopheles coluzzii* orthologous to the one used to drive salivary gland-specific transgene
180 expression in *Anopheles stephensi* (Yoshida and Watanabe, 2006). For both *saglin* and *trio*,
181 we defined putative promoter regions according to the genomic context. In addition, we also
182 used CRISPR/Cas9 to integrate a fluorescence cassette encoding EGFP into the endogenous
183 *saglin* locus, replacing the coding sequence, to study *saglin* promoter activity in its native
184 genomic context. Indeed, the activity of the cloned promoter selected for ectopic expression
185 was not ensured due to the shortness of the apparent *saglin* promoter region (220bp, **Fig. 1 –**
186 **figure supplement 2**). For this, site directed knock-in mutagenesis was performed by
187 injecting a plasmid encoding three guide RNAs targeting *saglin* and carrying a repair template
188 marked with *3xP3*-EGFP into mosquito eggs from a line with germline-specific expression of
189 Cas9 (*vasa-Cas9*), generating a *sag(-)KI* line (**Fig. 1B, Fig. 1 – figure supplement 3A**). To
190 place the *EGFP* gene directly under control of the *saglin* promoter, the *3xP3* promoter used to
191 selected transgenic mosquito larvae was flanked by lox sites to enable its excision by Cre
192 recombination (**Fig. 1 – figure supplement 3A**, Material & Methods). Similarly, we
193 generated a knockin (KI) into the *yellow* gene that encodes a protein required for the synthesis
194 of black pigments in insects (Hunt and Bridges, 1916; Wittkopp, True and Carroll, 2002). For
195 this, we used a plasmid with guide RNAs specific for *yellow* and corresponding homology
196 arms flanking a fluorescence cassette expressing *EGFP* surrounded by lox sites (**Fig. 1 –**
197 **figure supplement 3B**). Through crossing of salivary gland reporter lines with low
198 pigmented *yellow(-)KI* mosquitoes, we aimed to improve the fluorescence signal of the
199 expressed reporter and extend the range of applications, e.g. for *in vivo* imaging. Genotyping
200 by PCR confirmed the successful generation of the salivary gland reporter lines *aapp-DsRed*,

201 *aapp-hGrx1-roGFP2*, *trio-DsRed* and *sag-DsRed* (**Fig 1 – figure supplement 1B**) as well as
202 the mosquito lines *sag(-)KI* and *yellow(-)KI* (**Fig. 1 – figure supplement 3C,D**). Loss of the
203 *3xP3* promoter in *sag(-)EX* mosquitoes (mosquitoes lacking the *3xP3* promoter after *Cre*
204 mediated excision) was confirmed by PCR in the progeny of a cross between the *sag(-)KI* line
205 and a mosquito line expressing *Cre* recombinase in the germline (**Fig. 1 – figure supplement**
206 **3E**) (Volohonsky *et al.*, 2015).
207
208 **Lobe-specific transcriptional activation by *sag*, *aapp* and *trio* promoter sequences**
209 Dissection of female salivary glands revealed a highly specific expression pattern of DsRed,
210 EGFP and hGrx1-roGFP2 driven by *sag, aapp* and *trio* promoter sequences inside salivary
211 glands (**Fig. 1C**). While no fluorescence was observed for DsRed driven by the cloned 5'
212 upstream sequence of the *saglin* gene in dissected salivary glands (**Fig. 1 – figure**
213 **supplement 2A**), promoter activity was detected in the line where *EGFP* replaced the *saglin*
214 gene (**Fig. 1C**), indicating that essential transcriptional elements localize outside of the
215 intergenic sequence between *AGAP000609* and *AGAP000610* (*saglin*) (**Fig. 1 – figure**
216 **supplement 2B**). Interestingly, fluorescence signals in glands of female *aapp-DsRed*, *aapp-*
217 *hGrx1-roGFP2* mosquitoes were restricted to the distal-lateral lobes, while female *trio-DsRed*
218 and *sag(-)EX* mosquitoes displayed fluorescence exclusively in the median lobe (**Fig. 1C**).
219 This difference became especially evident when crossing *aapp-hGrx1-roGFP2* mosquitoes
220 with *trio-DsRed* mosquitoes giving rise to a trans-heterozygous offspring displaying hGrx1-
221 roGFP2 expression in distal-lateral lobes combined with DsRed expression in the median lobe
222 (**Fig. 1C**). Similarly, when crossing *aapp* and *trio* DsRed reporter lines, the entire salivary
223 gland was red fluorescent in the F1 progeny (**Fig. 1C**). Expression of *trio-DsRed* and *aapp-*
224 *DsRed* was so strong that the respective parts of the salivary gland appeared pink colored
225 even in brightfield microscopy (**Fig. 1C**). Of note, fluorescent reporter expression in the
226 salivary glands of *aapp-DsRed*, *aapp-hGrx1-roGFP2* and *trio-DsRed* mosquito colonies was
227 restricted to females while no fluorescence signal could be observed in this organ in males
228 (**Fig. 2 – figure supplement 1A**). Imaging of *aapp-DsRedP*, *aapp-hGrx1-roGFP2* and *trio-*
229 *DsRed* pupae during development revealed no distinct fluorescence signal in the head part
230 where the salivary glands are located (**Fig. 2 – figure supplement 1B**). Still, *DsRed*
231 expression was visible in the salivary glands of *aapp-DsRed* females that had been dissected
232 directly after emergence (**Fig. 2A**), indicating that the *aapp* promoter is already active in
233 pharate adults. In contrast, no *DsRed* expression was observed in the glands of freshly
234 hatched *trio-DsRed* females (**Fig. 2A**). To evaluate the expression profile over time we

235 performed a time-course experiment by dissecting and imaging salivary glands of *trio-DsRed*
236 and *aapp-DsRed* females every day. *DsRed* expression guided by *aapp* and *trio* promoters
237 increases steadily until day 5 after hatching (**Fig. 2B**). The increase in *DsRed* expression over
238 time in the salivary glands of *aapp-DsRed* and *trio-DsRed* females could also be followed in
239 transmitted light based on the pink coloration of the distal-lateral lobes (**Fig. 2 – figure**
240 **supplement 1C**). In *Anopheles stephensi, AAPP* expression was shown by qRT-PCR to be
241 upregulated upon blood feeding (Yoshida and Watanabe, 2006). We followed DsRed
242 fluorescence levels in the salivary glands of *aapp-DsRed* and *trio-DsRed* sibling mosquitoes
243 that were fed on blood or kept on sugar (**Fig. 2C,D**). Our results confirm that the *aapp*
244 promoter is induced upon ingestion of a blood meal while there was no difference between
245 blood-fed and sugar-fed in females expressing the *trio-DsRed* transgene.
246
247 **Spatial expression pattern of the *saglin* and *trio* promoters in the median lobe**
248 While expression of the fluorescent probes *DsRed* and *hGrx1-roGFP2* in the mosquito lines
249 *aapp-DsRed*, *trio-DsRed* and *aapp-DsRed* is driven by the cloned *aapp* and *trio* promoter
250 sequences, the selection of transgenic *sag(-)KI* larvae required the use of the synthetic *3xP3*
251 promoter to allow expression of *EGFP* in neonate larvae. To assess the activity of the native
252 *saglin* promoter, the *3xP3* promoter was flanked by lox sites that allowed its excision using
253 Cre to generate the *sag(-)EX* line (**Fig. 1 – figure supplement 3).** Imaging of salivary glands
254 (dissected tissues or through the cuticle in live mosquitoes) from *sag(-)KI* and *sag(-)EX*
255 females revealed that *EGFP* expression is much stronger in specimens expressing the *sag(-*
256 *)KI* transgene, indicating that the synthetic *3xP3* promoter enhances the native transcriptional
257 activity of the *saglin* promoter (**Fig. 3A**). As for the *aapp* promoter, reporter expression in
258 *Sag(-)EX* was detected in salivary glands of mosquitoes that had just emerged (**Fig. 2A**), and
259 increased after blood feeding (**Fig. 2C,D**). Of note, EGFP signal was 1.8 and 2.6 fold stronger
260 at the base than at the apex of the median lobe of the salivary gland in *sag(-)KI* and *sag(-)EX*
261 females, respectively (**Fig. 3A,B**). The mean fluorescence of *sag(-)KI* was 5.5-fold and 3.8-
262 fold higher than that of *sag(-)EX* at the apex and base, respectively (**Fig. 3B**). Next, we
263 crossed *sag(-)KI* and *aapp-trio* mosquitoes. Confocal imaging of salivary glands dissected
264 from heterozygous individuals expressing both transgenes revealed a striking difference in the
265 expression pattern of the *trio* and *saglin* promoters. *DsRed* expression driven by *trio* was
266 observed strongest in the apex of the median lobe with low to no expression in cells of the
267 base (**Fig. 3C,D**). In contrast *EGFP* expression driven by the *saglin* promoter was detectable
268 along the median lobe in an opposite gradient as described above (**Fig. 3B,D**). Imaging of the

269 base of a gland expressing *aapp-DsRed* and *sag(-)KI* showed a remarkably sharp expression
270 boundary between cells with high and low *saglin* promoter activity. Only few high producer
271 cells close to the boundary were observed to co-express *aapp-DsRed* (**Fig. 3E**). Using z-
272 stacks of confocal images from dissected *sag(-)KI* salivary glands stained with Hoechst 33342,
273 we further determined that the median lobe consists of 144 cells on average of which 49 cells
274 display high and 95 low *saglin* promoter activity. Considering the observed differences in the
275 mean fluorescence between apex and base and assuming that the expression of *EGFP*
276 represents the expression of *saglin*, cells at the base of the median lobe contribute ~88% to
277 Saglin expression, while the cells in the apex contribute only ~12%, although the apex area
278 contains nearly twice as many cells as the base.
279
280 **Subcellular localization of fluorescent reporters**
281 During first microscopic examinations using low magnification, different intracellular
282 localizations of the fluorescent proteins DsRed, EGFP and hGrx1-roGFP2 were observed (**Fig.**
283 **1C**), which was confirmed by confocal microscopy. DsRed expressed in the salivary glands
284 of *aapp-DsRed* and *trio-DsRed* mosquitoes appeared spotty and displayed a vesicle-like
285 pattern within the cytoplasm of the acinar cells, while hGrx1-roGFP2 and EGFP expressed in
286 the glands of *aapp-hGrx1-roGFP2* and *sag(-)EX* mosquitoes displayed a more cytoplasmic
287 localization (**Fig. 4**). Due to the anatomy of the secretory cells, which form an inward cavity
288 into which saliva is secreted, the vesicle-like DsRed accumulations localized mainly at the
289 outer rim of the salivary gland. In contrast, localization of hGrx1-roGFP2 and EGFP was
290 homogenous in the cytoplasm but appeared to be enriched around nuclei (**Fig. 4 – figure**
291 **supplement 1**).
292
293 **Variation of DsRed expression in *trio-DsRed* mosquitoes**
294 During the generation of the salivary gland reporter lines and their subsequent outcrossing we
295 observed that most L1 mosquito larvae carrying the *trio-DsRed* transgene displayed
296 fluorescence in the eyes (**Fig. 5A**), which was absent in the two other reporter lines *aapp-*
297 *DsRed* and *aapp-hGrx1-roGFP2*. Interestingly, a few L4 stage larvae of the *trio-DsRed* line
298 even displayed strong ubiquitous *DsRed* expression (**Fig. 5A**). At the pupal stage, *DsRed*
299 expression was detected in the ocellus, an eye spot close to the main compound eye, the
300 antennae and/or throughout the body. The observed expression patterns were highly variable
301 and ranged from completely non-fluorescent pupae to pupae expressing *DsRed* in all three
302 tissues (**Fig. 5 – figure supplement 1A**). In adult mosquitoes, DsRed signal was less distinct

303 compared to pupae although complete body fluorescence was occasionally observed in both
304 males and females, with the strongest expression of *DsRed* in the salivary glands of females
305 and the palps and antennae of males (**Fig. 5B**). Dissections of adult mosquitoes displaying
306 whole body fluorescence at the pupal stage revealed strong and sex-independent DsRed
307 signals in Malphigian tubules, an insect organ that performs functions similar to the vertebrate
308 kidney (**Fig. 5C**). Of note, fluorescence in tubules strictly correlated to the high pupal
309 fluorescence phenotype and was never observed in mosquitoes hatched from low fluorescent
310 pupae (**Fig. 5D**). We next investigated sex-specificity of each fluorescence pattern at the
311 pupal stage and inheritance of the high and low fluorescent *trio-DsRed* transgene. Non-
312 fluorescent pupae were always females, while fluorescent antennae were observed exclusively
313 in male pupae (**Fig. 5 – figure supplement 1B**). In contrast, the presence of a fluorescent
314 ocellus or body fluorescence was sex-independent. Quantification of the observed expression
315 pattern revealed that a fluorescent ocellus, either alone or in combination with body
316 fluorescence, was most frequently observed, and that the ratio of pupae that displayed body
317 fluorescence to those that did not was close to 50% (**Fig. 5 – figure supplement 1C**). To
318 follow the inheritance pattern of high and low body fluorescence, pupae were separated
319 according to their fluorescence phenotype and intercrossed. Quantification of pupal *DsRed*
320 expression in the F1 generation revealed a strong enrichment for whole body fluorescence
321 (~80%) if high pupal body fluorescence was selected in the previous generation. In contrast,
322 no pupae with high body fluorescence were observed in the offspring of mosquitoes hatched
323 from low fluorescent pupae (**Fig. 5 – figure supplement 1D**). This result is consistent with
324 Mendelian inheritance, with the locus conferring high body fluorescence being dominant over
325 that conferring low body fluorescence. To investigate this further, virgin female pupae of the
326 F1 generation displaying high pupal *DsRed* expression were crossed with wild type males.
327 Ten single female families were created which were all screened for pupal body fluorescence.
328 All families except family 8 displayed a 1:1 distribution for high and low pupal body
329 fluorescence (**Fig. 5 – figure supplement 1E**). Family 8 displayed exclusively high pupal
330 body fluorescence, indicating that the founder female was homozygous for the locus
331 conferring high body fluorescence, while all other females were heterozygous for the
332 „low“ and the „high“ *trio-DsRed* loci. Notably, we detected high DsRed signals in the
333 salivary glands of all adult females in families 5, 6, 7, 8 and 10 (other families were not
334 investigated), regardless of whether individuals hatched from pupae displaying high or low
335 body fluorescence. Genotyping of females homozygous for low *trio-DsRed* and heterozygous

336 for WT/high *trio-DsRed* revealed a single integration of the transgene into the X1 locus as
337 expected (**Fig. 5 – figure supplement 2**).
338
339 **Glutathione redox state and morphology of acinar cells expressing hGrx1-roGFP2**
340 To assess the redox sensitivity of hGrx1-roGFP2 expressed in the *aapp-hGrx1-roGFP2* line,
341 salivary glands were dissected and treated either with diamide or dithiothreiol to oxidize or
342 reduce the fluorescent probe, respectively. As control, salivary glands were treated with N-
343 ethyl-maleimide to preserve the native redox state of the dissected tissue. Samples were
344 imaged at 405 and 488 nm and the ratio of both wavelengths was plotted (**Fig. 6A**), revealing
345 a dynamic range of 4.2 between fully oxidized and fully reduced probes (**Fig. 6B**).
346 Interestingly, the ratio of native salivary glands was very similar to measurements performed
347 on samples treated with dithiothreiol (Red), suggesting that the glutathione pool is largely
348 reduced in acinar cells (**Fig. 6B**). Infection with *P. berghei* sporozoites did not affect the
349 redox state of salivary glands (**Fig. 6C**). Of note, initial imaging experiments pointed towards
350 a thinning of the tips of the distal-lateral lobes in salivary glands expressing *aapp-hGrx1-*
351 *roGFP2,* while glands obtained from *aapp-DsRed*, *trio-DsRed* and *sag(-)KI* or *sag(-)EX*
352 females appeared similar to wild type (**Fig. 1, Fig. 6D**). Measurement of the diameter at the
353 "neck-region" of the distal-lateral lobes confirmed its thinning in salivary glands expressing
354 *aapp-hGrx1-roGFP2* compared to wild type and *aapp-DsRed* (**Fig. 6E**). This difference is
355 likely due to a flattening of the cell body of the acinar cells within the tips, which was
356 observed by confocal microscopy. (**Fig. 4**).
357
358 **Salivary gland reporter lines as a tool to investigate sporozoite interactions with salivary**
359 **glands**
360 We next investigated whether our highly fluorescent salivary gland reporter lines could
361 facilitate *in vivo* imaging of *Plasmodium* development through the cuticle of a living
362 mosquito using the a *GFP* expressing parasite strain (*Δp230p-GFP)* of the rodent malaria
363 parasite *P. berghei* (**Fig. 7A**) (Manzoni *et al.*, 2014). This strain is bright enough to make
364 parasites visible through the mosquito cuticle, allowing pre-sorting of infected mosquitoes
365 based on fluorescence in the mosquito midgut, the salivary glands and the wing joint, a
366 localization where hemolymph sporozoites tend to accumulate. To test if the expression of a
367 fluorescent reporter in the salivary glands alters parasite development in the mosquito, we
368 infected the three reporter lines *trio-DsRed*, *aapp-DsRed* and *aapp-hGrx1-roGFP2* as well as
369 the parental line *G3*. Parasite counts observed in reporter lines varied from 118 to 142 oocysts

370 and were not significantly different from controls (121 oocysts) (**Fig. 7 – figure supplement**
371 **1A**). The average number of salivary gland sporozoites at day 17-18 after infection was 8.200
372 to 17.400 sporozoites per mosquito in salivary gland reporter lines vs 9.600 in *G3* controls
373 (**Fig. 7 – figure supplement 1B**). An average of 10.000 salivary gland sporozoites per
374 mosquito is usually observed in our laboratory, with numbers fluctuating from 5.000 to more
375 than 20.000 sporozoites per mosquito in non-transgenic lines, indicating no significant
376 difference between the *G3* control and reporter lines. To normalize the counts of salivary
377 gland sporozoites relative to differences in oocyst numbers, we calculated the number of
378 sporozoites that had successfully invaded the salivary glands per oocyst. Again, no significant
379 difference was detected between reporter lines (86-146 sporozoites per oocyst) and *G3* control
380 (133) mosquitoes (**Fig. 7 – figure supplement 1C**). To assess if the *3xP3* driven expression
381 of EGFP in the low pigmented *yellow(-)KI* line would interfere with the imaging of GFP
382 positive *P. berghei* parasites, adult *yellow(-)KI* and WT females were imaged in the GFP
383 channel to compare emitted fluorescence signals (**Fig. 7 – figure supplement 1D**). *Yellow(-*
384 *)KI* females showed a weak GFP signal in the head and, suprisingly, strongly fluorescent
385 ovaries. While gene expression within parts of the eye and the nervous system of the head is
386 typical for the expression pattern of the *3xP3* promoter in mosquitoes, EGFP expression in the
387 ovaries is likely due to the endogenous promoter activity of the *yellow* promoter. However, no
388 significant increase in green fluorescence was observed at the throat area where the salivary
389 glands localize compared with WT, suggesting that imaging of GFP-positive parasites would
390 be feasible.
391 While the expression of a fluorescence reporter makes it simple to detect the location of the
392 salivary glands through the cuticle, light absorption by pigments and light scattering by chitin
393 generate signal losses reducing image quality and resolution. To reduce light absorption, we
394 crossed *aapp-DsRed* mosquitoes, displaying highly fluorescent salivary glands without
395 altered morphology, with *yellow(-)KI* mosquitoes (**Fig. 7A,B**). Yellow is a protein required
396 for the synthesis of black pigments in insects, its absence renders the cuticle pale and
397 yellowish (Hunt and Bridges, 1916; Wittkopp, True and Carroll, 2002). As expected, *yellow(-*
398 *);aapp-DsRed* mosquitoes displayed a low pigmented cuticle in combination with highly
399 fluorescent salivary glands (**Fig. 7B**). The decrease in pigmentation greatly increased the
400 observed GFP signal visible through the cuticle, notably in strongly pigmented areas that
401 appear almost black in WT mosquitoes (**Fig. 7C**). We also investigated whether GFP- or
402 mCherry-positive sporozoites can be imaged in fluorescent salivary glands. Live imaging of
403 dissected infected glands showed that fluorescent sporozoites can be clearly distinguished

404 from the fluorescent signal of salivary glands at low magnification while lobe-specific
405 fluorescence expression allowed for simple differentiation between median and distal-lateral
406 lobes (**Fig. 7D**). In addition, imaging showed that all salivary gland reporter lines may have a
407 high sporozoite load, suggesting that fluorescence expression in salivary glands does not
408 affect individual salivary gland sporozoite colonization.
409 We next imaged mosquitoes infected with *P. berghei Δp230p-GFP* between day 17 and day
410 20 after infection, when sporozoites invade the salivary glands. Mosquitoes were pre-sorted
411 for GFP fluorescence in the salivary glands (**Fig. 7 – figure supplement 2A**) as well as in the
412 wing joint (not shown) to confirm the presence of sporozoites. In a subset of mosquitoes (less
413 than 1 out of 5), we observed that the salivary glands localized very close to the cuticle **(Fig. 7**
414 **– figure supplement 2B,C**). To facilitate *in vivo* imaging, we further selected mosquitoes
415 positive for sporozoites and with cuticular localization of at least one salivary gland and
416 prepared them for imaging (**Fig. 7 – figure supplement 2D**). Confocal imaging enabled to
417 visualize precisely single sporozoites through the cuticle close to the salivary gland as well as
418 subcellular structures, like the cavities of acinar cells, of the gland itself (**Fig. 8A**). However,
419 we noted that a significant portion of the DsRed signal was also seen in the GFP channel,
420 especially at lower magnification, suggesting a possible spillover of the DsRed signal. This
421 could possibly occur due to the concentration difference between DsRed in the acinar cells
422 and EGFP in the sporozoites (**Fig. 7-figure supplement 2E**). Nevertheless, spillover effects
423 did not affect detection of sporozoites at higher magnification, and quantification of the
424 recorded films revealed that ~26% of persistent sporozoites were (at least 5 minutes in the
425 field of view) in the thorax area perform pattern of active movement while ~19% are attached
426 but not moving and ~55% are floating (**Fig. 8A**). The observed movement patterns resembled
427 in most cases the patch gliding previously described *in vitro*. During this type of movement,
428 sporozoite adheres in the center and performs jerky back-and-forth movements along its
429 adhesive patch (**Fig. 8B, Movies 1 and 2**) (Münter *et al.*, 2009; Klug *et al.*, 2020). Due to the
430 brevity of the recorded movies (5 minutes), many actively moving sporozoites appeared to
431 remain on the site without making large terrain gains. However, in some cases, the position of
432 the adhesive patch was observed to change slightly over time, such that sporozoites made
433 small terrain gains in one direction while continuously sliding back and forth. Importantly, we
434 were also able to observe sporozoites inside salivary glands (**Fig, 8C**).
435
436
437

438 ## Discussion

439 Mosquito salivary glands have long interested entomologists, parasitologists, virologists and
440 microbiologists because they are a key organ in the transmission of vector borne diseases.
441 Still, the host-pathogen interactions that allow the specific recognition and colonization of this
442 organ by different pathogens has been understudied, probably in part because of the relative
443 difficulty to access and visualize these processes in comparison to midgut invasion. The
444 reporter lines we generated in this study represent valuable tools to circumvent some of these
445 issues: they enable (1) easy visualization of the glands, even in brightfield or DIC microscopy,
446 (2) distinguishing distal-lateral and median lobes of the salivary glands, and (3) imaging of
447 single sporozoites in proximity to and inside salivary glands *in vivo*.

448 We used the promoters of three salivary gland genes, *aapp*, *trio* and *saglin*, to drive
449 fluorescent reporter expression in *A. coluzzii* mosquitoes. The different fluorescence patterns
450 obtained in the salivary glands of these lines show that the proteomes of median and distal-
451 lateral lobes are diverse and most likely contribute different saliva components. In addition,
452 the variable fluorescence intensity in the distal-lateral lobes of both *aapp* lines (stronger
453 towards the apex) point towards an even more complex expression pattern along the lobe.
454 This hierarchical expression was even more evident for the *trio* and *saglin* promoters, both of
455 which are active in the median lobe but with opposite expression patterns. *saglin* is strongly
456 active in cells at the base and less active in the apex, in contrast, *trio* expression is absent in
457 cells with high *saglin* activity, but very strong in cells with low *saglin* activity. While the
458 expression pattern of *trio* has not been investigated before, the observed activity of the *saglin*
459 promoter is coherent with immunofluorescence studies performed in *A. stephensi* (O'Brochta
460 *et al.*, 2019). Expression of *saglin* in the median lobe is puzzling since the protein has been
461 shown to affect colonization of the salivary glands by *Plasmodium* sporozoites, (Ghosh and
462 Jacobs-Lorena, 2009), whereas parasites prefer to invade the distal-lateral lobes (Wells and
463 Andrew, 2019) that lack activity of the *saglin* promoter. A possible explanation is that the site
464 of expression of both proteins is not the site where they interact with parasites.

465 The absence of reporter expression in mosquitoes expressing *DsRed* controlled by the *saglin* 5'
466 upstream sequence is likely due to the shortness of the cloned sequence. The *saglin* gene
467 localizes in the middle of an array of four genes believed to be salivary gland-specific
468 (Francischetti *et al.*, 2002) and separated by short intergenic regions (**Fig. 1 – figure**
469 **supplement 2**). Regulatory sequences controlling transcription are likely located upstream
470 and/or downstream of this array and might be shared by all four genes.

471 Notably, the reporter lines display different subcellular localizations of hGrx1-roGFP2, EGFP
472 and DsRed. While all expressed fluorescent proteins lack any targeting signal which could
473 explain a different localization, only hGrx1-roGFP2 (*aapp*) and EGFP (*saglin*) localized
474 within the cytoplasm. In contrast, DsRed displayed a vesicular pattern in both the median
475 (*trio*) and the distal-lateral lobes (*aapp*), while a DsRed2 variant driven by the *aapp* promoter
476 in *A. stephensi* mosquitoes was shown to be cytoplasmic (Yoshida and Watanabe, 2006).
477 Although AAPP was shown previously to localize in a vesicle-like fashion (Wells, Villamor
478 and Andrew, 2017), we believe that the observed localization differences are likely not based
479 on putative artefactual trafficking signals. First, vesicular localization of DsRed was observed
480 with both the *trio* and *aapp* promoters, and second, only DsRed appeared vesicular, whereas
481 hGrx1-roGFP2 was cytoplasmically localized, although both proteins were expressed from
482 the same *aapp* sequence. Comparison of the DsRed sequence used here with the previously
483 described DsRed2 sequence expressed in *A. stephensi* revealed mutations mainly in the N-
484 terminal region and the addition of 11 unrelated amino acids at the C-terminus of DsRed2
485 (Yoshida and Watanabe, 2006). It is likely that these sequence differences between the two
486 DsRed versions lead to the formation of a cryptic trafficking signal recognized by the acinar
487 cells. Interestingly, although we did not investigate their nature, we also observed the
488 presence of vesicles in the salivary glands of wild type mosquitoes with similar distribution
489 and morphology and displaying weak red autofluorescence (**Fig. 1 – figure supplement 2**).
490 DsRed could potentially be trafficked to these or similar compartments explaining its unique
491 localization. Differences in salivary gland morphology between *aapp-DsRed* and *aapp-*
492 *hGrx1-roGFP2* expressing mosquitoes are likely due to the expression of human
493 Glutaredoxin 1 (hGrx1) and not of roGFP2, a protein derived from EGFP with 2 amino acid
494 changes. Indeed, no change in morphology was detected in *sag(-)EX* and *sag(-)KI* mosquitoes
495 expressing EGFP alone in the median lobe. Still, EGFP appeared less expressed in *sag(-)EX*
496 compared to hGrx1-roGFP2 in *aapp-hGrx1-roGFP2* (**Fig. 1**) and we cannot exclude that the
497 acinar cells of the median and distal-lateral lobes react differently to the expression of the
498 respective reporters, or that the cells show different responses to roGFP2 and EGFP. Despite
499 its influence on cell morphology, the salivary glands of hGrx1-roGFP2 expressing mosquitoes
500 retained their integrity even in old mosquitoes and apoptosis of cells expressing the
501 fluorescent reporter was not observed.
502 We also report a surprisingly large panel of fluorescence patterns in mosquitoes expressing
503 the *trio-DsRed* transgene. The *trio* promoter activated transcription of DsRed in the salivary
504 glands of all females (but not in males), but also in ocelli, antennae and Malpighian tubules as

505 well as whole body in some but not all mosquitoes, independently of their sex but for
506 antennae that were strictly restricted to males, and with a strict correlation between strong
507 *DsRed* expression in pupal body and adult Malpighian tubules. The fact that *trio* expression
508 was reported to be salivary gland-specific (Dragovic *et al.*, 2018) suggests that the region we
509 selected upstream of *trio* does not contain all regulatory elements that control its natural
510 expression, or that the genomic context of the X1 locus may influence its expression. To date,
511 the number of available promoters able to drive ubiquitous expression of transgenes in
512 *Anopheles* mosquitoes is limited (Adolfi *et al.*, 2018), thus replacing DsRed in a selected
513 highly fluorescent line could provide a new means to ubiquitously express transgenes. By
514 sorting and crossing according to the observed pupal fluorescence phenotype, it was possible
515 to separate alleles conferring high and low pupal body fluorescence, which allowed the
516 production of a colony enriched with the high pupal fluorescence phenotype and a colony
517 showing only low pupal body fluorescence. This observation pointed towards a genetically
518 encoded difference which is inherited in a Mendelian manner rather than a transient
519 (epi)genetic modification. Genotyping confirmed the presence of a single copy of the
520 transgene in the X1 locus in both lowly and highly fluorescent mosquitoes. Since fluorescent
521 ocelli, antennae and whole body expression were only observed in the *trio-DsRed* population,
522 we propose that the different *DsRed* expression patterns are locus-specific variegation effects
523 caused by interactions between the selected *trio* promoter sequence and polymorphic
524 regulatory elements that could be linked or unlinked to the transgene. Although unlikely, we
525 cannot rule out the possibility that some mosquitoes carried an extra copy of the transgene
526 that caused the highly fluorescent phenotype. Still, DsRed positive ocelli and antennae were
527 observed in both high and low fluorescence populations, which is most likely explained by a
528 variable *DsRed* expression from the transgene inserted at X1. While the observed *DsRed*
529 expression patterns in larvae and pupae are helpful in the laboratory to select transgenic
530 individuals, it also urges caution in interpreting results as it clearly shows that transcription is
531 contextual.
532 Intravital imaging has revealed the dynamics of parasite development inside its vertebrate
533 host (Sturm *et al.*, 2006; Wang *et al.*, 2020). While optical windows in mice is a well
534 implemented method (De Niz *et al.*, 2019), *in vivo* imaging through the cuticle of insects is
535 rarely performed, mostly because it is difficult to achieve good resolution by imaging through
536 the insect cuticle that scatters and absorbs light. Recent studies have explored the possibility
537 to circumvent this issue through the application of clearing protocols on infected mosquitoes
538 to improve resolution and enable imaging through whole mosquitoes (Mori, Hirai and Mita,

539 2019; De Niz *et al.*, 2020). However, while these improvements are remarkable, imaging of
540 cleared specimens only represents snapshots whereas mapping of dynamic processes are
541 desirable. Imaging of tissues *ex vivo* in combination with the use of hemolymph-like media
542 allows the observation of dynamic processes (Klug and Frischknecht, 2017). Still, imaging *ex*
543 *vivo* samples can only be performed for a limited amount of time and artifacts due to the
544 artificial tissue environment cannot be excluded. A step towards intravital imaging was made
545 recently by developing a protocol that combines feeding of dyes relevant for imaging with
546 blood feeding prior to sample preparation (Trisnadi and Barillas-Mury, 2020). Due to the
547 inflation of the mosquito abdomen directly after feeding, cuticle plates open up and create
548 temporary optical windows that can be exploited for microscopy. Still, in this case,
549 mosquitoes were decapitated and tightly flattened between microscopy slide and cover slip,
550 thus allowing for optimal imaging but maintaining *in vivo* conditions only for a limited time.
551 To demonstrate the use of the salivary gland reporter lines for imaging purposes, we crossed
552 *aapp-DsRed* mosquitoes with the weakly pigmented mosquito line *yellow(-)KI* deficient for
553 black pigment synthesis. In a subset of mosquitoes, salivary glands localized very closely to
554 the cuticle allowing the recognition of subcellular structures of the gland in living mosquitoes.
555 In addition, the more transparent cuticle allowed better visibility of individual sporozoites
556 through the cuticle. It is generally believed that sporozoites, after they have been released
557 from the oocyst, are passively transported to the salivary glands and engage in active motility
558 only upon contact with acinar cells (Douglas *et al.*, 2015). Our *in vivo* observations show that
559 ~26% of persistent thorax sporozoites perform active motility mostly in a patch gliding
560 manner (**Movie 1** and **2**) (Münter *et al.*, 2009; Klug *et al.*, 2020). This could be an indication
561 that the motility of the sporozoites is already crucial to reach the salivary glands and ensure
562 efficient colonization. Testing mutants that produce immobile sporozoites could provide more
563 sophisticated information on the extent to which sporozoite motility promotes invasion of
564 salivary glands.
565 Here we provide a proof of concept of *in vivo* salivary gland imaging, and we hope that the
566 method can be further improved to gain a better insight in the invasion process of salivary
567 glands by sporozoites. Potential spillover effects of the DsRed signal in salivary glands of
568 *aapp-DsRed* females could possibly be avoided by using a *P. berghei* reporter line with
569 stronger GFP expression (Natarajan *et al.*, 2001). Furthermore the injection of fluorescent
570 beads or dyes could be used as vitality measure to monitor the active movement of the
571 hemolymph while, at the same time, highlighting contact areas with hemolymph and salivary
572 glands. Also, we did not exhaust the repertoire of possible genetic modifications to decrease

573 pigmentation of the cuticle. Deletion of the genes *tan* and *ebony*, two enzymes which regulate
574 the homeostasis of the pigment precursors dopamine and N-ß-alanyldopamine, in
575 combination with the deletion of *yellow* could potentially further decrease cuticle
576 pigmentation (Wittkopp, True and Carroll, 2002; True *et al.*, 2005). Another possibility could
577 be the overexpression of arylalkylamine-*N*-acetyltransferase, an enzyme converting dopamine
578 into the sclerotizing precursor molecule N-acetyldopamine, which was shown to affect
579 pigmentation in different insect species by enhancing the production of colorless components
580 of the cuticle (Osanai-Futahashi *et al.*, 2012). A key improvement for *in vivo* imaging would
581 be an increase in the number of mosquitoes displaying ideally positioned salivary glands.
582 Preliminary monitoring experiments showed that the position of the gland does not
583 significantly change over time in adult mosquitoes indicating that positioning occurs during
584 metamorphosis. Should salivary gland positioning be genetically determined, selective
585 breeding may help to improve the ratio of mosquitoes with cuticular salivary glands. Taken
586 together, we hope that the transgenic lines developed in this study can contribute to improve
587 *in vivo* imaging and salivary gland dissections in *Anopheles* mosquitoes, and enable real-time
588 imaging of *Plasmodium* and other vector borne pathogens.
589

Key Resources Table				
Reagent type (species) or resource	**Designation**	**Source or reference**	**Identifiers**	**Additional information**
strain, (*Escherichia coli*)	*DH5h*	self made	/	Chemically competent cells
Strain, (*Anopheles coluzzii*)	*X1*	(Volohonsky *et al.*, 2015)	/	attP docking line
Strain, (*Anopheles coluzzii*)	*vasa-Cas9*	(Keller Valsecchi *et al.*, 2021)	/	Strain with germline-specific Cas9 expression
Strain, (*Anopheles coluzzii*)	*Ngousso*	MR4	MRA-1279	Wild type strain
Strain, (*Anopheles coluzzii*)	*G3*	/	/	Wild type strain
Strain, (*Anopheles coluzzii*)	*aapp-DsRed*	this study	/	DsRed expression in distal lobes
Strain, (*Anopheles coluzzii*)	*trio-DsRed*	this study	/	DsRed expression in median lobe

Strain, (*Anopheles coluzzii*)	*aapp-hGrx1-roGFP2*	this study	/	hGrx1-roGFP2 expression in distal lobes
Strain, (*Anopheles coluzzii*)	*sag-DsRed*	this study	/	No DsRed expression
Strain, (*Anopheles coluzzii*)	*sag(-)KI*	this study	/	Knockin into Saglin expressing EGFP from 3xP3 promoter
Strain, (*Anopheles coluzzii*)	*sag(-)EX*	this study	/	Knockin into Saglin with excised 3xP3 promoter
Strain, (*Mus musculus*)	*CD-1*	Janvier Labs	/	self-bred
Strain, (*Plasmodium berghei*)	*Δp230p-GFP*	(Manzoni *et al.*, 2014)	/	Constitutive expression of GFP
Strain, (*Plasmodium berghei*)	*Δp230p-mCherry*	(Manzoni *et al.*, 2014)	/	Constitutive expression of mCherry
Recombinant DNA reagent	*pENTR R4 ATCC LacZ GCTT*	(Volohonsky *et al.*, 2015)	Addgene: #1773668	/

Recombinant DNA reagent	*pDSAP*	(Volohonsky *et al.*, 2015)	Addgene: #62293	/
Recombinant DNA reagent	P1 / P44, aapp 5'UTR forward	this study	Primer	GGTCTCGATCCCTTTTCTTTTACCCTTTGTAACACGCTAATAACG
Recombinant DNA reagent	P2, aapp 5'UTR reverse	this study	Primer	GGTCTCGCTCTGTCGTTTTTTGTTGTTGTGGTATTATTTCACTG
Recombinant DNA reagent	P3 / P46, hGrx1-roGFP2 forward	this study	Primer	GGTCTCGAGAGATGGCTCAAGAGTTTGTGAACTGCAAAATC
Recombinant DNA reagent	P4, hGrx1-roGFP2 reverse	this study	Primer	GGTCTCGAAGCTTACTTGTACAGCTCGTCCATGCCG
Recombinant DNA reagent	P5, DsRed aapp / trio forward	this study	Primer	GGTCTCGAGAGATGGTGCGCTCCTCCAAGAACG
Recombinant DNA reagent	P6, DsRed aapp / trio reverse	this study	Primer	GGTCTCGAAGCCTACAGGAACAGGTGGTGGCGGC
Recombinant DNA reagent	P7 / P45, trio 5'UTR forward	this study	Primer	GGTCTCGATCCTTTTCTGAGGTGATCTTTCGAAAAGATCG

Recombinant DNA reagent	P8, trio 5'UTR reverse	this study	Primer	GGTCTCGCTCTGTAACTGGGAGCAGATTGATTTTATGG
Recombinant DNA reagent	P9 / P42, saglin 5'UTR forward	this study	Primer	GGTCTCGATCCCTTTCATGCGTACAATGTGTATGATCACTG
Recombinant DNA reagent	P10, saglin 5'UTR reverse	this study	Primer	CGTTCTTGGAGGAGCGCACCATTTATAAGTGAACCTTATGCAAACCTTCCCTG
Recombinant DNA reagent	P11 / P40, DsRed saglin forward	this study	Primer	CAGGGAAGGTTTGCATAAGGTTCACTTATAAATGGTGCGCTCCTCCAAGAACG
Recombinant DNA reagent	P12, DsRed saglin reverse	this study	Primer	GGTCTCGAAGCCTACAGGAACAGGTGGTGGCGG
Recombinant DNA reagent	P13, Yellow gRNA1 forward	this study	Oligonucleotide	CCTTGTAGCGTGCCTGGTGGCCGC
Recombinant DNA reagent	P14, Yellow gRNA1 reverse	this study	Oligonucleotide	AAACGCGGCCACCAGGCACGCTAC
Recombinant DNA reagent	P15, Yellow gRNA2 forward	this study	Oligonucleotide	CCTTGGCGACTACGTGCCCACGAA

Recombinant DNA reagent	P16, Yellow gRNA2 reverse	this study	Oligonucleotide	AAACTTCG TGGGCACG TAGTCGCC
Recombinant DNA reagent	P17, Yellow gRNA3 forward	this study	Oligonucleotide	CCTTGGAG AACAAGCT GTTCGTCT
Recombinant DNA reagent	P18, Yellow gRNA3 reverse	this study	Oligonucleotide	AAACAGAC GAACAGCT TGTTCTCC
Recombinant DNA reagent	P19 / P33, Yellow 5'UTR forward	this study	Primer	GGTCTCGA ACAGAATT GAACGCCC AAGGTACG GCTG
Recombinant DNA reagent	P20 / P34, Yellow 5'UTR reverse	this study	Primer	GGTCTCAC CCCGCTTC TGCCACTA AGGAACTT CTGTG
Recombinant DNA reagent	P21, Yellow 3'UTR forward	this study	Primer	GGTCTCGA AGACGTGT GTCCTGGA AGTGTGAT TTATCG
Recombinant DNA reagent	P22, Yellow 3'UTR reverse	this study	Primer	GGTCTCGA AGCGTAGC GTGCCTGG TGGCCGCC GGAACGCT TTCCCTGC AGCGTAC
Recombinant DNA reagent	P23, Saglin gRNA1 forward	this study	Oligonucleotide	CCTTGCGT TCAAGTCA TCTCGAGC

Recombinant DNA reagent	P24, Saglin gRNA1 reverse	this study	Oligonucleotide	AAACGCTCGAGATGACTTGAACGC
Recombinant DNA reagent	P25, Saglin gRNA2 forward	this study	Oligonucleotide	CCTTGCCGCAGTCCTCGCGGCTGG
Recombinant DNA reagent	P26, Saglin gRNA2 reverse	this study	Oligonucleotide	AAACCCAGCCGCGAGGACTGCGGC
Recombinant DNA reagent	P27, Saglin gRNA3 forward	this study	Oligonucleotide	CCTTGAAGTTTGCAACGTTTGCGA
Recombinant DNA reagent	P28, Saglin gRNA3 reverse	this study	Oligonucleotide	AAACTCGCAAACGTTGCAAACTTC
Recombinant DNA reagent	P29, Saglin 5'UTR forward	this study	Primer	GGTCTCGAACATGGGTTCACTCGCTGTTAGACTGTG
Recombinant DNA reagent	P30, Saglin 5'UTR reverse	this study	Primer	GGTCTCAATGGTTATAAGTGAACCTTATGCAAACCTTCCCTG
Recombinant DNA reagent	P31, Saglin 3'UTR forward	this study	Primer	GGTCTCGAAGAGCGTCGGCGACGGTCTAAAAG

Recombinant DNA reagent	P32, Saglin 3'UTR reverse	this study	Primer	GGTCTCGA AGCGTTCA AGTCATCT CGAGCCGG CTTCTTCT GCTGCCGC AGAAAC
Recombinant DNA reagent	P35, X1 forward 1	this study	Primer	CCCGTCAT GAGTTCAA GCCTGAA
Recombinant DNA reagent	P36, attB reverse	this study	Primer	CCCGGTCT CAAATTGC CCGCCGTG ACCGTCGA
Recombinant DNA reagent	P37, OpiE2 forward	this study	Primer	CAAGCACC TTTATACTC GGTGGCCT C
Recombinant DNA reagent	P38, PuroR reverse 1	this study	Primer	TTCCAGGA AGGCGGG CACCCC
Recombinant DNA reagent	P39, X1 reverse	this study	Primer	ACTGCAAC CCATTCAC ACTG
Recombinant DNA reagent	P41, SV40 reverse	this study	Primer	CCTCTACA AATGTGGT ATGGCTGA
Recombinant DNA reagent	P43, X1 forward 2	this study	Primer	CCTTGAAG ATTGGAAT CCATCCAT

Recombinant DNA reagent	P47, Saglin 5' forward genotyping	this study	Primer	GCTTATAAGAGCGCTACGGGTGTAC
Recombinant DNA reagent	P48, Saglin 3' reverse genotyping	this study	Primer	CTGTCCCTTCAGCTTCACCAGCTC
Recombinant DNA reagent	P49, Yellow 5' forward genotyping	this study	Primer	GAACGACAGGTGAGCTGACAGTAAC
Recombinant DNA reagent	P50, Yellow 3' reverse genotyping	this study	Primer	GATTTGGCGAGATGGTTTGTGCGAC
Recombinant DNA reagent	P51, PuroR reverse 2	this study	Primer	GAGCTCGAGTTCAGGCACCGGGCTTGC
Recombinant DNA reagent	P52, EGFP reverse	this study	Primer	CTTCGGGCATGGCGGACTTG
Recombinant DNA reagent	P53, SV40 forward	this study	Primer	CAGCCATACCACATTTGTAGAG
Commercial assay or kit	CloneJET PCR Cloning Kit	ThermoFisher Scientific	Cat#K1231	/
Software, algorithm	Prism 5.0	GraphPad, San Diego, US	/	https://www.graphpad.com/scientific-software/prism/

Software, algorithm	FIJI	(Schindelin *et al.*, 2012)	/	https://imagej.net/software/fiji/
Software, algorithm	MetaMorph	Molecular Devices, San Jose, US	/	https://www.moleculardevices.com/contact
Software, algorithm	VectorBase (version 36-55)	(Amos *et al.*, 2022)	/	https://vectorbase.org/vectorbase/app
Software, algorithm	NIS-Elements, F 4.20.01, 64 Bit	Nikon Instruments Inc., Melville, US	/	https://www.microscope.healthcare.nikon.com/products/software/nis-elements
Software, algorithm	DNAStar Lasergene, SeqBuilder Pro	DNASTAR, Madison, US	/	https://www.dnastar.com/
Other	Hoechst 33342	ThermoFisher Scientific	Cat#H3570	/

592 ## Materials & methods

593

594 **Animals**

595 Transgenesis was performed in the *Anopheles coluzzii* strain X1 (Volohonsky *et al.*, 2015) or
596 in a strain expressing Cas9 from the X1 locus under control of the *vasa* promoter
597 (transgenesis plasmid: Addgene # 173670) and introgressed into the *Ngousso* genetic
598 background. Wild type *Anopheles coluzzii* strains *Ngousso* and *G3* were used as controls.
599 CD1 mice purchased from Charles River or from our own colonies were used for both
600 mosquito maintenance through blood meals, and for parasite maintenance and mosquito
601 infections. For infections with rodent malaria parasites, we made use of the *Plasmodium*
602 *berghei* line *Δ p230p-GFP* derived from the wild type background *P. berghei ANKA*
603 (Manzoni *et al.*, 2015).

604

605 **Breeding of mosquitoes**

606 *Anopheles coluzzii* mosquitoes were kept in standard conditions (27°C, 75-80% humidity, 12-
607 hr/12-hr light/dark cycle). Larvae were hatched in pans of osmosed water and fed with
608 pulverized fish food (TetraMin, Melle, Germany). Adult mosquitoes were maintained on a
609 10% sucrose solution. To propagate colonies, four to seven-day old mosquitoes were blood
610 fed for 10-15 minutes on anesthetized mice and allowed to lay eggs on wet filter paper 2-3
611 days later. For mosquito blood feeding, female CD-1 mice (> 35g) were anesthetized with a
612 mixture of Zoletil (42.5 mg/kg) and Rompun (8.5 mg/kg) in 0.9% NaCl solution.

613

614 **Construction of salivary gland reporter transgenes**

615 The 5'upstream sequences of *saglin* (primers P9 and P10), *aapp* (primers P1 and P2) and *trio*
616 (primers P7 and P8) were amplified from genomic DNA of *G3* mosquitoes isolated with the
617 Blood & Tissue Kit (Qiagen) as shown in **File S1**. DsRed (primers P5 and P6 for *aapp/trio*;
618 P11 and P12 for *saglin*) and hGrx1-roGFP2 (primers P3 and P4) were amplified from the
619 plasmids pJET-DsRed-SV40 and pDSAP_actin-hGrx1-roGFP2 (donated by Raquel Mela-
620 Lopez). Primers are shown in **Table S1**. PCR was performed using Phusion polymerase
621 according to the manufacturer recommendations (ThermoFisher Scientific) and subcloned in
622 the pJET vector using the CloneJET PCR Cloning Kit (ThermoFisher Scientific). The
623 5'upstream sequence of the *saglin* gene was fused to the *DsRed* gene by a Phusion mediated
624 assembly PCR (TerMaat *et al.*, 2009) before cloning into pJET. After sequence verification,

625 assembly blocks were fused into the destination vector pDSAP (Volohonsky et al., 2015,
626 Addgene # 62293) using Goldengate cloning and generating pDSAP-aapp-DsRed, pDSAP-
627 aapp-hGrx1-roGFP2, pDSAP-trio-DsRed and pDSAP-saglin-DsRed.
628
629 **Construct cloning for site-directed mutagenesis into *yellow* and *saglin* genes**
630 For the design of guide RNAs (gRNAs), the coding sequence of *saglin* as well as the first
631 exon of the *yellow* gene were manually searched for PAMs (NGG), with N representing any
632 nucleotide. Candidate gRNA sequences were investigated for potential off-target effects using
633 http://www.rgenome.net/cas-designer/ (Cas-OFFinder) (Bae, Park and Kim, 2014). We
634 selected gRNAs starting with a G considering the transcription start from the U6 promoter
635 and differing by ≥3 nucleotides from putative off-target sequences in the *A. coluzzii* genome.
636 For each knockin construct, linkers encoding the protospacer motif of three gRNAs (**Table**
637 **S1**) were generated by annealing two primers ordered from IDT DNA and cloned using *BbsI*
638 into pKSB-sgRNA (Addgene #173671—3) vectors containing the U6 snRNA polymerase III
639 promoter (AGAP013557), the invariable sequence of a standard crRNA-tracerRNA fusion
640 (Jinek et al., 2012), and the RNA polIII TTTTT terminator. The three complete gRNAs
641 blocks were then assembled into a single pKSB-sgRNA destination plasmid by GoldenGate
642 cloning using different but matching *BsaI* overhangs. For the construction of repair templates,
643 regions of homology on the 5' side (*saglin*: primers P29 and P30; *yellow*: primers P19 and
644 P20) and on the 3' side (*saglin*: primers P31 and P32; *yellow*: primers P21 and P22) of the
645 region targeted by the gRNAs were amplified from *Ngousso* genomic DNA and subcloned in
646 the pJET vector, generating plasmids pJET-5'saglin, pJET-5'yellow, pJET-3'saglin and
647 pJET-3'yellow. After sequence validation, all building blocks were fused in the correct order
648 in the destination plasmid pENTR using GoldenGate assembly together with a building block
649 containing either the fluorescence cassette pKSB-Lox3xP3Lox-EGFP or pKSB-Lox3xP3-
650 EGFP-Lox, generating pENTR-Saglin;Lox3xP3Lox-EGFP and pENTR-Yellow;Lox3xP3-
651 EGFP-Lox. Primers are shown in **Table S1**.
652
653 **Transgenesis of *A. coluzzii***
654 All plasmids used for DNA injections were purified using Endofree kits (Qiagen). Freshly
655 laid eggs of the docking line X1 or the *vasa-Cas9* line were injected as described (Fuchs,
656 Nolan and Crisanti, 2013; Pondeville *et al.*, 2014; Volohonsky *et al.*, 2015). For ΦC31-
657 integrase mediated transgenesis a mix of three plasmids (pDSAP-aapp-DsRed, pDSAP-aapp-
658 hGrx1-roGFP2 and pDSAP-trio-DsRed) (~160 ng/µL) and the integrase helper plasmid

659 carrying the Vasa2-ΦC31-Integrase gene (Addgene # 62299, ~200 ng/µL) diluted in 0.5x
660 phosphate buffered saline (0.1 mM NaHPO4 buffer, 5 mM KCl, pH 6.8) was injected into
661 approximately 500 embryos. The plasmid pDSAP-saglin-DsRed was injected in the same
662 way but into a different batch of eggs. For site-directed knock-in mediated by Cas9, the
663 plasmid solution (pENTR-Saglin;Lox3xP3Lox-EGFP or pENTR-Yellow;Lox3xP3Lox-
664 EGFP) (~200-300 ng/µL) was diluted in PBS supplemented with 1 µM Scr7 to inhibit non-
665 homologous end joining. Each construct was injected in a separate batch of approximately
666 500 eggs obtained from *vasa-Cas9* females.
667
668 **Salivary gland reporter lines *sag-DsRed, trio-DsRed, aapp-DsRed* and *aapp-hGrx1-***
669 ***roGFP2***
670 Following egg micro-injection, surviving pupae were sorted according to sex, hatched in
671 separate cages (G0 generation) and crossed with ~100 mosquitoes of the other sex from a
672 mosquito line expressing CFP from the X1 docking site that was used as a balancer of the
673 new, non-fluorescent but puromycin resistant transgenic insertions at the same locus. Neonate
674 larvae from this cross were treated with puromycin (0.05 mg/mL). G1 pupae were
675 subsequently sex sorted and crossed with CFP positive mosquitoes to expand the population.
676 Adult puromycin resistant G2 females were sorted according to the observed fluorescence
677 phenotype (DsRed or roGFP2) in their salivary glands, reflecting the expression of the *trio-*
678 *DsRed*, *aapp-DsRed* or *aapp-hGrx1-roGFP2* transgenes and crossed to CFP balancer males.
679 For *sag-DsRed* females, sorting was not necessary, as transgenesis was performed separately
680 by injection of the pDSAP-saglin-DsRed plasmid alone. Puromycin-resistant G3 larvae were
681 raised, intercrossed and the G4 offspring was sorted by COPAS (Marois et al., 2012) for the
682 absence of CFP to select lines homozygous for *sag-DsRed*, *trio-DsRed*, *aapp-DsRed* and
683 *aapp-hGrx1-roGFP2*. Lines were then raised without puromycin treatment. Single females of
684 all generated colonies were genotyped by PCR to monitor correct integration of the transgene
685 into the docking site (**Fig. S1A,B**). Successfully genotyped mosquito colonies were expanded
686 and used to perform experiments.
687
688 ***yellow(-)KI* and *sag(-)KI* lines**
689 Pupae obtained from plasmid injected eggs were sorted according to sex and crossed with 100
690 *Ngousso* wild type partners. G1 neonate larvae were screened for the expression of EGFP
691 using a Nikon SMZ18 fluorescence Stereomicroscope. Selected transgenic larvae were sex
692 sorted at the pupal stage and crossed with an excess of wild type partners. The G2 progenies

693 (from a single positive G1 female for *sag(-)KI* and from 10 positive individuals for *yellow(-*
694 *)KI*) were COPAS sorted to enrich for the integrated transgene and to remove the *vasa-Cas9*
695 transgene (marked with DsRed). The generated *sag(-)KI* colony was kept in equilibrium with
696 the wild type allele, while the *yellow(-)KI* colony was completely homozygotized for the
697 transgene by selecting for mosquitoes with a yellow body color. Homozygous *sag(-)KI*
698 mosquitoes were crossed with the C2S line expressing Cre in the germline (Volohonsky *et al.*,
699 2015) for Cre recombinase-mediated excision of the lox cassette to generate *sag(-)EX*
700 mosquitoes.
701
702 **Genotyping of mosquito lines**
703 Genotyping was performed on genomic DNA extracted from single mosquitoes of *aapp-*
704 *DsRed*, *aapp-hGrx1-roGFP2*, *trio-DsRed*, *sag(-)KI, sag(-)EX* and *yellow(-)KI* colonies.
705 Genotyping PCRs were performed using GoTaq Green Mastermix (Promega) (**Fig. S1B**),
706 Phusion polymerase (ThermoFisher Scientific) or the Phire Tissue Direct PCR Master Mix
707 (ThermoFisher Scientific) (**Fig. S2** and **S7**) according to manufacturer recommendations. See
708 **Table S2** for genotyping primers.
709
710 **Mosquito infection and evaluation of parasite numbers**
711 Parasites were maintained as frozen stocks at -80ºC or by passage between mice. For this,
712 blood was taken by heart puncture from a donor mouse with a parasitaemia of 3-5%, diluted
713 to 2.10^7 parasitized erythrocytes in 100 µL 0.9% NaCl that were injected intravenously into a
714 naïve mouse. Parasitemia was monitored via flow cytometry (Accuri C6, BD biosciences)
715 three days later. Mosquitoes were fed for 10-15 min on anesthetized mice with 2.5 – 3.5%
716 parasitemia. Blood fed females were sorted and kept on 10% sucrose at 21ºC and 50-70%
717 humidity. Midguts and salivary glands were dissected in PBS under a SZM-2 Zoom
718 Trinocular stereomicroscope (Optika). Images were acquired with the Nikon SMZ18
719 Stereomicroscope (without coverslip) or with a Zeiss LSM 780 confocal microscope (sealed
720 coverslip). To count oocysts, midguts were dissected 7-8 days post infection. Fluorescence
721 images of infected midguts were processed using the watershed segmentation plugin (Soille
722 and Vincent, 1990) and oocysts were subsequently counted using the „analyze
723 particles“ function implemented in Fiji (Schindelin *et al.*, 2012). To count salivary gland
724 sporozoites, salivary glands were collected in PBS 17-18 days post infection and ground with
725 a plastic pestle for one minute. The number of sporozoites was measured using a Neubauer

726 hemocytometer under a light microscope (Zeiss).
727
728 **Fluorescence imaging, fluorescence measurements and image analysis**
729 Samples imaged using the Nikon SMZ18 Stereomicroscope were usually acquired using the
730 respective fluorescence filter to visualize expression of DsRed or roGFP2/EGFP combined
731 with brightfield to visualize the whole specimen. Images were taken using a 63-fold
732 magnification objective (NA 1.4) on a Zeiss LSM 780 confocal microscope (**Fig. 3A**), a
733 Zeiss Axiovert 200 fluorescence microscope **(Fig. S2A**) or using an iPhone 6 for the mounted
734 mosquitoes prepared for microscopy in **Fig. S8D**. All other images as well as images used for
735 fluorescence measurements were acquired with a Nikon SMZ18 Stereomicroscope. For
736 fluorescence quantifications, images were acquired in the DsRed channel and settings were
737 kept the same for all experiments. For each salivary gland, only a single lobe was measured
738 by analyzing a square of 51×51 pixels covering the central part of the fluorescent area to
739 determine the mean fluorescence intensity. The image processing for all experiments was
740 performed with Fiji (Schindelin *et al.*, 2012).
741
742 **roGFP measurements**
743 Dissected salivary glands were treated as in (Albrecht *et al.*, 2011). In brief, tissues were
744 alkylated in 20 mM N-ethyl-maleimide (NEM) for 15 min to preserve the redox state of
745 roGFP and then fixed in paraformaldehyde (4% PFA) for 20 min. In parallel, full oxidation
746 and reduction controls were prepared by incubating some samples in 2 mM diamide or 20
747 mM dithiotreitol (DTT), respectively, prior to alkylation with NEM and fixation as described
748 before. All compounds were prepared in phosphate-buffered saline. Salivary glands were
749 mounted with VectaShield (Vector Laboratories) and samples were stored at 4°C in the dark
750 until analysis. Samples were imaged with a Zeiss Axio Observer Z1 confocal LSM780
751 microscope by using a Plan-Apochromat 63x/1.4 oil objective. The expressed fluorescent
752 probe hGrx1-roGFP2 was excited sequentially at 405 and 488 nm, and its emission signal was
753 recorded at 500-530 nm. Images were processed in ImageJ following the protocol described
754 in (Kardash, Bandemer and Raz, 2011). In brief, background was subtracted by using the
755 rolling ball procedure set to 50 pixels and images were converted to 32-bit. Then, images
756 were smoothed and stacked. The intensity of the 488 nm image was thresholded with the
757 default settings in black and white; values below threshold were set to "not a number". The
758 ratio image was generated by dividing the 405 nm picture by the 488 nm picture using the

759 “Ratio Plus” plugin, and colored using the lookup table “fire”. Subsequently, intensities were
760 normalized to the DTT control.
761
762 ***In vivo* imaging**
763 For *in vivo* imaging experiments, infected *yellow(-);aapp-DsRed* mosquitoes were pre-
764 screened between days 17 - 21 post infection for the presence sporozoites (GFP fluorescence)
765 in the hemolymph (hinge of the wing) and salivary glands, as well as for cuticular positioning
766 of the salivary gland (DsRed signal) (**Fig. 7 – Supplement 2**). After removing their legs,
767 mosquitoes were glued on a microscopy slide using small amounts of UV-light reactive glue
768 (Bondic Pocket) and covered with a coverslip prepared with plasticine feet at each corner to
769 prevent a squeezing of the sample. Corners of the cover slip were coated with nail polish to
770 prevent sliding. Imaging was performed on a Zeiss Axio Observer Z1 confocal LSM780
771 microscope with GaAsP detector using a Plan-Apochromat 63x/1.4 oil objective. Single
772 images or movies of sporozoites and salivary glands were acquired with a duration of 5
773 minutes and 2 seconds per image using the Metamorph acquisition software.
774
775 **Statistical analysis**
776 Statistical analysis was performed using GraphPad Prism 5.0 (GraphPad, San Diego, CA,
777 USA). Data sets were either tested with a one-way ANOVA or a Mann Whitney test. A value
778 of $p<0.05$ was considered significant.
779
780 **Data availability**
781 All data have been made available within this manuscript. Transgenic mosquito lines as well
782 as plasmids are available upon request.
783
784 **Ethics statement**
785 Experiments were carried out in conformity with the 2010/63/EU directive of the European
786 Parliament on the protection of animals used for scientific purposes. Our animal care facility
787 received agreement #I-67-482-2 from the veterinary services of the département du Bas Rhin
788 (Direction Départementale de la Protection des Populations). The use of animals for this
789 project was authorized by the French ministry of higher education, research and innovation
790 under the number APAFIS#20562- 2019050313288887 v3. The generation and use of
791 transgenic lines (bacteria, mosquitoes, parasite) was authorized by the French ministry of
792 higher education, research and innovation under the number 3243.

Funding

This work was supported by the Laboratoire d'Excellence (LabEx) ParaFrap (grant LabEx ParaFrap ANR-11-LABX-0024), by the Equipement d'Excellence (EquipEx) I2MC (grant ANR-11-EQPX-0022), by the ERC Starting Grant Nº260918, and by funding from CNRS, Inserm, and the University of Strasbourg. DK is funded by a DFG postdoctoral fellowship (KL 3251/1-1).

Acknowledgements

We thank Amandine Gautier for help with rearing mosquitoes and technical assistance during infections with *P. berghei*, Sarra Manai for help with experiments, Jean-Daniel Fauny for assistance during microscopy and the whole mosquito immune responses (MIR) team for assistance with mosquito breeding and pupae collection.

Authors contributions

DK designed and performed experiments, analyzed data, made figures and wrote the draft. KA cloned constructs, performed initial experiments and analyzed data. EM performed transgenesis of mosquitoes. SB edited the draft and helped with conceptualization of experiments. All authors edited and approved the manuscript for publication.

Competing interests

The authors declare no competing interests.

References

Adolfi, A. *et al.* (2018) 'Multi-tissue GAL4-mediated gene expression in all Anopheles gambiae life stages using an endogenous polyubiquitin promoter', *Insect Biochemistry and Molecular Biology*. doi: 10.1016/j.ibmb.2018.03.005.

Albrecht, S. C. *et al.* (2011) 'In Vivo Mapping of Hydrogen Peroxide and Oxidized Glutathione Reveals Chemical and Regional Specificity of Redox Homeostasis', *Cell Metabolism*. Elsevier, 14(6), pp. 819–829. doi: 10.1016/j.cmet.2011.10.010.

Amos, B. *et al.* (2022) 'VEuPathDB: the eukaryotic pathogen, vector and host bioinformatics resource center', *Nucleic Acids Research*, 50(D1), pp. D898–D911. doi: 10.1093/nar/gkab929.

Arcà, B. *et al.* (2005) 'An updated catalogue of salivary gland transcripts in the adult female mosquito, Anopheles gambiae', *Journal of Experimental Biology*. doi: 10.1242/jeb.01849.

Bae, S., Park, J. and Kim, J. S. (2014) 'Cas-OFFinder: A fast and versatile algorithm that searches for potential off-target sites of Cas9 RNA-guided endonucleases', *Bioinformatics*. doi: 10.1093/bioinformatics/btu048.

Bhatt, S. *et al.* (2015) 'The effect of malaria control on Plasmodium falciparum in Africa between 2000 and 2015', *Nature*. doi: 10.1038/nature15535.

Calvo, E. *et al.* (2010) 'Aegyptin displays high-affinity for the von Willebrand factor binding site (RGQOGVMGF) in collagen and inhibits carotid thrombus formation in vivo', *The FEBS journal*. 2009/12/15, 277(2), pp. 413–427. doi: 10.1111/j.1742-4658.2009.07494.x.

Chuang, Y.-M. *et al.* (2019) 'Anopheles gambiae Lacking AgTRIO Inefficiently Transmits Plasmodium berghei to Mice', *Infection and immunity*. American Society for Microbiology, 87(9), pp. e00326-19. doi: 10.1128/IAI.00326-19.

Douglas, R. G. *et al.* (2015) 'Active migration and passive transport of malaria parasites', *Trends in Parasitology*, pp. 357–362. doi: 10.1016/j.pt.2015.04.010.

Dragovic, S. M. *et al.* (2018) 'Immunization with AgTRIO, a Protein in Anopheles Saliva, Contributes to Protection against Plasmodium Infection in Mice', *Cell Host and Microbe*. doi: 10.1016/j.chom.2018.03.008.

Figueiredo, A. C. *et al.* (2012) 'Unique thrombin inhibition mechanism by anophelin, an anticoagulant from the malaria vector', *Proceedings of the National Academy of Sciences of the United States of America*. 2012/12/05. National Academy of Sciences, 109(52), pp. E3649–E3658. doi: 10.1073/pnas.1211614109.

Francischetti, I. M. B. *et al.* (2002) 'Toward a catalog for the transcripts and proteins (sialome) from the salivary gland of the malaria vector Anopheles gambiae', *Journal of Experimental Biology*.

Fuchs, S., Nolan, T. and Crisanti, A. (2013) 'Mosquito transgenic technologies to reduce plasmodium transmission', *Methods in Molecular Biology*, 923, pp. 601–622. doi: 10.1007/978-1-62703-26-7_41.

Ghosh, A. K. *et al.* (2009) 'Malaria parasite invasion of the mosquito salivary gland requires interaction between the Plasmodium TRAP and the Anopheles saglin proteins', *PLoS Pathogens*, 5(1). doi: 10.1371/journal.ppat.1000265.

Ghosh, A. K. and Jacobs-Lorena, M. (2009) 'Plasmodium sporozoite invasion of the mosquito salivary gland', *Curr Opin Microbiol*, 12. doi: 10.1016/j.mib.2009.06.010.

Gutscher, M. *et al.* (2008) 'Real-time imaging of the intracellular glutathione redox potential', *Nature Methods*. doi: 10.1038/nmeth.1212.

Hayashi, H. *et al.* (2012) 'Anopheline anti-platelet protein from a malaria vector mosquito has anti-thrombotic effects in vivo without compromising hemostasis', *Thrombosis Research*. doi: 10.1016/j.thromres.2011.09.015.

Hunt, T. M. and Bridges, C. B. (1916) *Sex Linked Inheritance in Drosophila*, *Carnegie Institution of Washington*.

Juhn, J. *et al.* (2011) 'Spatial mapping of gene expression in the salivary glands of the dengue vector mosquito, Aedes aegypti', *Parasites & vectors*. BioMed Central, 4, p. 1. doi: 10.1186/1756-3305-4-1.

Kardash, E., Bandemer, J. and Raz, E. (2011) 'Imaging protein activity in live embryos using fluorescence resonance energy transfer biosensors', *Nature Protocols*, 6(12), pp. 1835–1846. doi: 10.1038/nprot.2011.395.

Keller Valsecchi, C. I. *et al.* (2021) 'Distinct mechanisms mediate X chromosome dosage compensation in Anopheles and <em>Drosophila</em&gt';, *Life Science Alliance*, 4(9), p. e202000996. doi: 10.26508/lsa.202000996.

Klug, D. *et al.* (2020) 'Evolutionarily distant I domains can functionally replace the essential ligandbinding domain of plasmodium trap', *eLife*. doi: 10.7554/eLife.57572.

Klug, D. and Frischknecht, F. (2017) 'Motility precedes egress of malaria parasites from oocysts', *eLife*, 6.

Manzoni, G. *et al.* (2014) 'A rapid and robust selection procedure for generating drug-selectable marker-free recombinant malaria parasites', *Scientific Reports*, 4(4760). doi: 10.1038/srep04760.

Manzoni, G. *et al.* (2015) 'A rapid and robust selection procedure for generating drug-selectable marker-free recombinant malaria parasites', *Scientific Reports*, 4(1), p. 4760. doi: 10.1038/srep04760.

Mori, T., Hirai, M. and Mita, T. (2019) 'See-through observation of malaria parasite behaviors in the mosquito vector', *Scientific Reports*. doi: 10.1038/s41598-019-38529-3.

Münter, S. *et al.* (2009) 'Plasmodium Sporozoite Motility Is Modulated by the Turnover of Discrete Adhesion Sites', *Cell Host and Microbe*, 6(6), pp. 551–562. doi: 10.1016/j.chom.2009.11.007.

Natarajan, R. *et al.* (2001) 'Fluorescent Plasmodium berghei sporozoites and pre-erythrocytic stages: A new tool to study mosquito and mammalian host interactions with malaria parasites', *Cellular Microbiology*, 3(6), pp. 371–379.

900 doi: 10.1046/j.1462-5822.2001.00117.x.
901 De Niz, M. *et al.* (2019) 'Intravital imaging of host–parasite interactions in skin
902 and adipose tissues', *Cellular Microbiology*. doi: 10.1111/cmi.13023.
903 De Niz, M. *et al.* (2020) '3D imaging of undissected optically cleared
904 Anopheles stephensi mosquitoes and midguts infected with Plasmodium
905 parasites', *PLOS ONE*. Public Library of Science, 15(9), p. e0238134.
906 O'Brochta, D. A. *et al.* (2019) 'Is Saglin a mosquito salivary gland receptor for
907 Plasmodium falciparum?', *Malaria Journal*. doi: 10.1186/s12936-018-2634-5.
908 Osanai-Futahashi, M. *et al.* (2012) 'A visible dominant marker for insect
909 transgenesis', *Nature Communications*. doi: 10.1038/ncomms2312.
910 Pondeville, E. *et al.* (2014) 'Efficient ΦC31 integrase–mediated site-specific
911 germline transformation of Anopheles gambiae', *Nature Protocols*, 9(7), pp.
912 1698–1712. doi: 10.1038/nprot.2014.117.
913 Salazar, M. I. *et al.* (2007) 'Dengue virus type 2: replication and tropisms in
914 orally infected Aedes aegypti mosquitoes', *BMC microbiology*. BioMed Central,
915 7, p. 9. doi: 10.1186/1471-2180-7-9.
916 Schindelin, J. *et al.* (2012) 'Fiji: an open-source platform for biological-image
917 analysis', *Nature Methods*, 9(7), pp. 676–682. doi: 10.1038/nmeth.2019.
918 Soille, P. and Vincent, L. M. (1990) '<title>Determining watersheds in digital
919 pictures via flooding simulations</title>', in *Visual Communications and Image
920 Processing '90: Fifth in a Series*. doi: 10.1117/12.24211.
921 Sturm, A. *et al.* (2006) 'Manipulation of host hepatocytes by the malaria parasite
922 for delivery into liver sinusoids.', *Science (New York, N.Y.)*, 313(5791), pp.
923 1287–1290. doi: 10.1126/science.1129720.
924 TerMaat, J. R. *et al.* (2009) 'Gene synthesis by integrated polymerase chain
925 assembly and PCR amplification using a high-speed thermocycler', *Journal of
926 Microbiological Methods*. doi: 10.1016/j.mimet.2009.09.015.
927 Trisnadi, N. and Barillas-Mury, C. (2020) ' Live In Vivo Imaging of
928 Plasmodium Invasion of the Mosquito Midgut ', *mSphere*. doi:
929 10.1128/msphere.00692-20.
930 True, J. R. *et al.* (2005) 'Drosophila tan encodes a novel hydrolase required in
931 pigmentation and vision.', *PLoS genetics*, 1(5). doi:
932 10.1371/journal.pgen.0010063.
933 Volohonsky, G. *et al.* (2015) 'Tools for Anopheles gambiae Transgenesis', *G3
934 (Bethesda); Genes|Genomes|Genetics*, 5(6), pp. 1151–1163. doi:
935 10.1534/g3.115.016808.
936 Wang, J. *et al.* (2013) 'Anopheles gambiae circumsporozoite protein-binding
937 protein facilitates plasmodium infection of mosquito salivary glands', *Journal of
938 Infectious Diseases*. doi: 10.1093/infdis/jit284.
939 Wang, L. T. *et al.* (2020) 'A Potent Anti-Malarial Human Monoclonal Antibody
940 Targets Circumsporozoite Protein Minor Repeats and Neutralizes Sporozoites in
941 the Liver', *Immunity*. doi: 10.1016/j.immuni.2020.08.014.
942 Wells, M. B. and Andrew, D. J. (2019) 'Anopheles salivary gland architecture

943 shapes plasmodium sporozoite availability for transmission', *mBio*. doi:
944 10.1128/mBio.01238-19.
945 Wells, M. B., Villamor, J. and Andrew, D. J. (2017) 'Salivary gland maturation
946 and duct formation in the African malaria mosquito Anopheles gambiae',
947 *Scientific Reports*, 7(1), p. 601. doi: 10.1038/s41598-017-00672-0.
948 Wittkopp, P. J., True, J. R. and Carroll, S. B. (2002) 'Reciprocal functions of the
949 Drosophila Yellow and Ebony proteins in the development and evolution of
950 pigment patterns', *Development*.
951 Yoshida, S. and Watanabe, H. (2006) 'Robust salivary gland-specific transgene
952 expression in Anopheles stephensi mosquito', *Insect Molecular Biology*. doi:
953 10.1111/j.1365-2583.2006.00645.x.
954

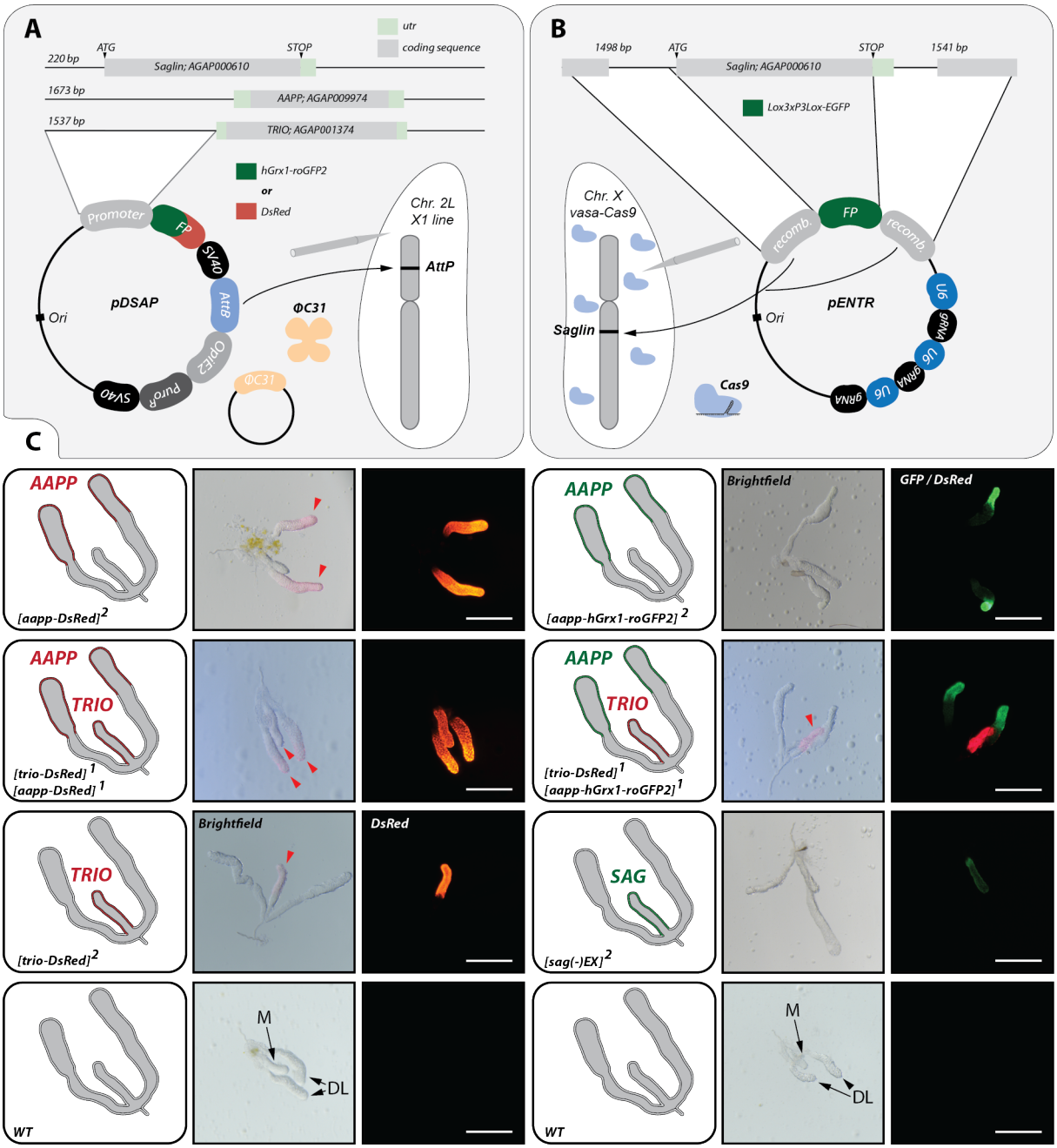

Figure 1. Lobe-specific reporter expression observed in female *aapp-DsRed*, *aapp-hGrx1-roGFP2*, *trio-DsRed* and *sag(-)EX* mosquitoes.
A) ΦC31 integrase-mediated transgene insertion. The *aapp*, *trio* and *saglin* promoter sequences were fused to *DsRed* or *hGrx1-roGFP2* within the pDSAP vector which enables chemical selection of mosquito larvae by puromycin. Transgenes were integrated by ΦC31 integrase-mediated recombination into the X1 line harbouring an *attP* site on chromosome 2L. **B)** Cas9-mediated knockin of a fluorescence cassette in the *saglin* gene (AGAP000610). Upstream and downstream sequences of *saglin* were cloned into the pENTR vector flanking a fluorescence cassette expressing *EGFP* under the control of the *3xP3* promoter. Three guides targeting *saglin* controlled by *U6* promoters were encoded on the same pENTR vector. Transgenesis was performed in mosquitoes with germline-specific expression of Cas9 (vasa-Cas9). **C)** Fluorescent reporter expression in mosquitoes homozygous for *trio-DsRed*, *aapp-DsRed*, *aapp-hGrx1-roGFP2* and *sag(-)EX* (*3xP3* promoter excised) as well as in females

970 heterozygous for *trio-DsRed* and *aapp-DsRed,* and *trio-DsRed* and *aapp-hGrx1-roGFP2.*
971 Salivary glands of wild type (*G3*) are shown as controls. Illustrations on the left of each panel
972 indicate the genotype of the gland as well as the observed fluorescence pattern. Images of
973 salivary glands are shown in brightfield beside an image of the same gland in the relevant
974 fluorescence channel. Red arrows in brightfield images highlight the pink parts of *aapp-*
975 *DsRed* and *trio-DsRed* salivary glands in the absence of fluorescence excitation indicating the
976 high expression of DsRed. Median (M) and distal-lateral lobes (DL) are indicated on the
977 images of wild type glands. Salivary glands were dissected from 2-10 day old females that
978 had not previously received blood feeding. Scale bars: 250 µm.
979

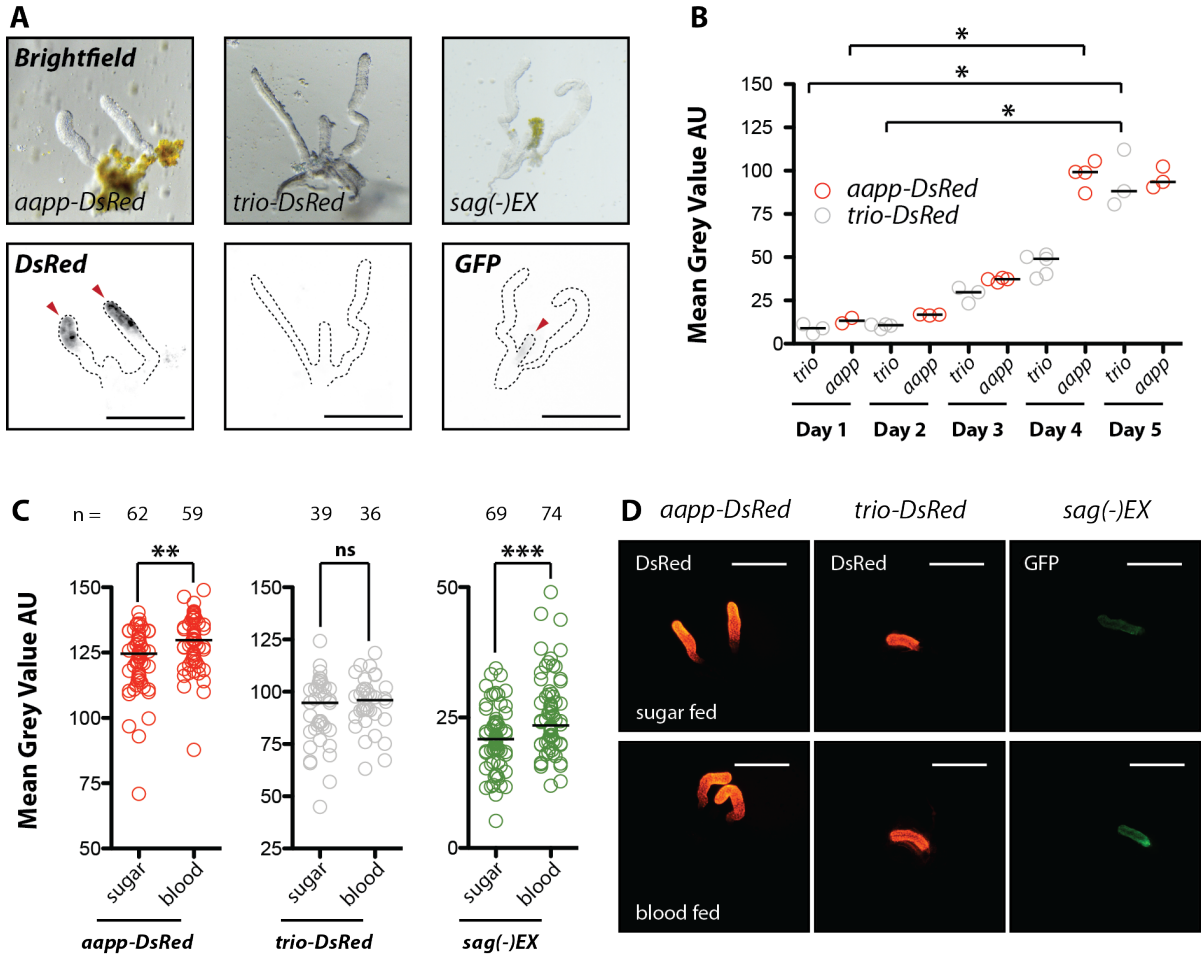

Figure 2. Onset, strength and inducibility by blood feeding of reporter expression in *aapp-DsRed*, *trio-DsRed* and *sag(-)EX* mosquitoes.
A) Images of salivary glands dissected directly after mosquitoes emerged. Fluorescence signals were observed in salivary glands expressing *aapp-DsRed* and *sag(-)EX* (marked by red arrowheads) but not *trio-DsRed*. Scale bar: 250 µm. **B)** Mean fluorescence intensity measurements of dissected *aapp-DsRed* and *trio-DsRed* salivary glands from day one to day five after hatching. Data were normalized for the highest exposure time. Each dot represents a single gland (2-5 glands / timepoint) and bars the median. *p<0.01, one-way-ANOVA (Dunn's Multiple Comparison Test). **C)** The blood meal inducibility of the *trio*, *aapp* and *saglin* promoters was assessed by providing sibling females either with a blood meal or sugar solution. Approximately 24h later, salivary glands were dissected, imaged and the mean DsRed or EGFP fluorescence intensities were quantified. Data pooled from three (*aapp-DsRed* and *trio-DsRed*) or four (*sag(-)EX*) independent experiments. Horizontal black bars represent the median. **p<0.001 and *** p<0.0001, Mann Whitney test. ns: not significant. **D)** Images of salivary glands dissected 24h after blood feeding in comparison to sugar fed controls. Scale bar: 250 µm.

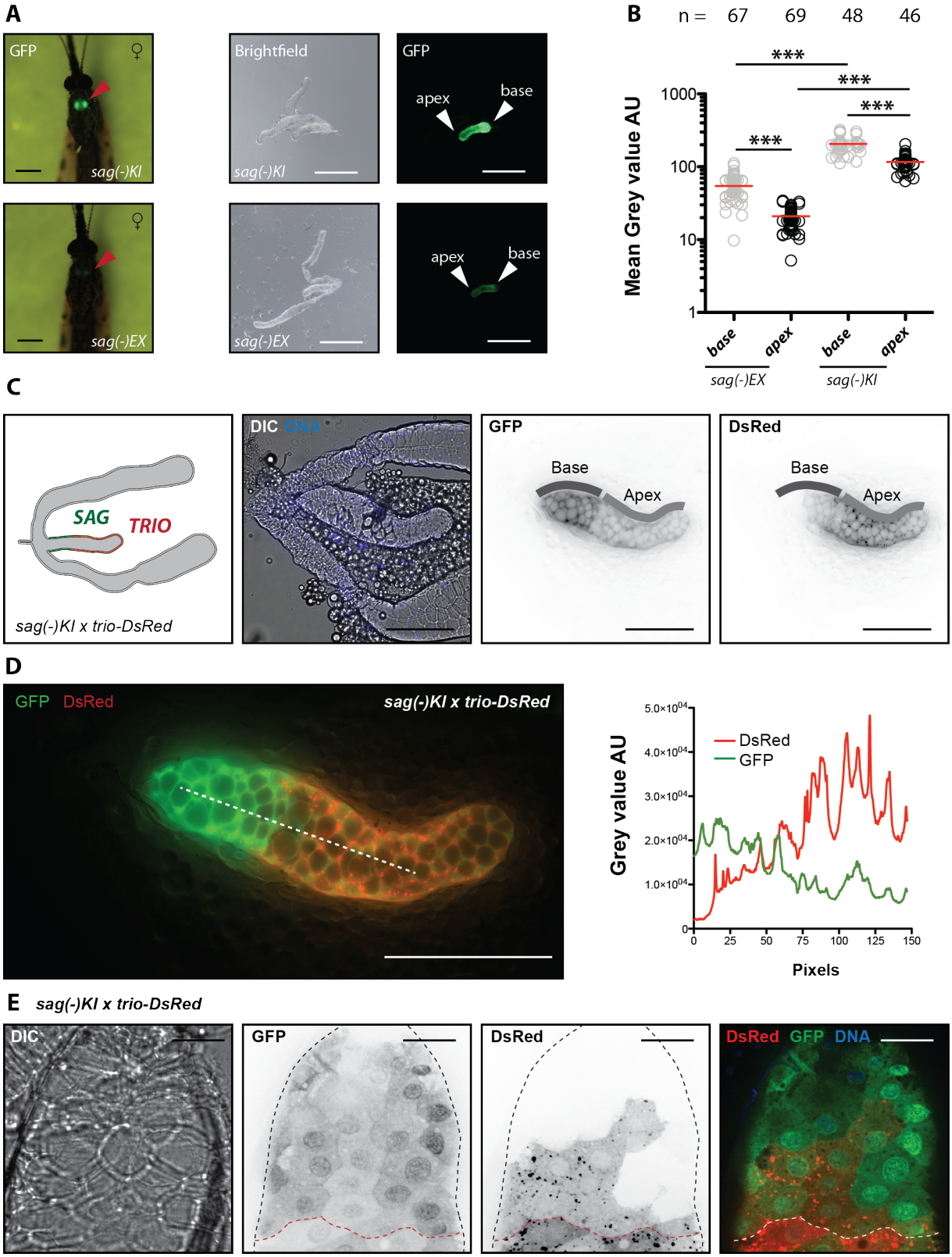

Figure 3. Fluorescent reporter expression in the median lobe reveals spatial expression differences of *saglin* and *trio* promoters.

A) *EGFP* expression in homozygous *sag(-)KI* and *sag(-)EX* females seven days after emergence (left side). Red arrows point towards the location of the salivary glands. Scale bar: 0.5 mm. Brightfield and GFP signal in dissected salivary glands of homozygous *sag(-)KI* and *sag(-)EX* females (right side). Positions of the base and apex of the median lobe are indicated.

1007 Scale bar: 250 µm. **B)** Mean EGFP fluorescence quantification at the apex and at the base of
1008 the median lobe of *sag(-)EX* and *sag(-)KI* salivary glands dissected after sugar feeding. The
1009 number of measured salivary glands is indicated above each column. Data from four (*sag(-*
1010 *)KI)* and three (*sag(-)EX*) experiments obtained from two different mosquito generations. The
1011 black line indicates the median. ***p<0.0001, one-way-ANOVA (Bonferroni's Multiple
1012 Comparison Test). **C)** Optical (C, D) and confocal (E) imaging of salivary gland heterozygous
1013 for *sag(-)KI* and *trio-DsRed*. Left to right (C): Illustration of the genotype and observed
1014 fluorescence pattern, differential interference contrast (DIC) and nuclear staining with
1015 Hoechst 33342, GFP signal and DsRed signal as black on white. Positions of the base and
1016 apex of the median lobe are indicated. Scale bar: 100 µm. **D)** Merge of the GFP and DsRed
1017 signals shown in (C). Line plot on the right shows measured GFP and DsRed signals along
1018 the dotted white line. Scale bar: 100 µm. **E)** Confocal imaging of a salivary gland
1019 heterozygous for *sag(-)KI* and *trio-DsRed*. The basal area of the median lobe is shown. The
1020 black dotted line indicates the outline of the salivary gland as seen in DIC while the red dotted
1021 line indicates the border between cells displaying high and low *saglin* promoter activity. Scale
1022 bar: 20 µm.
1023

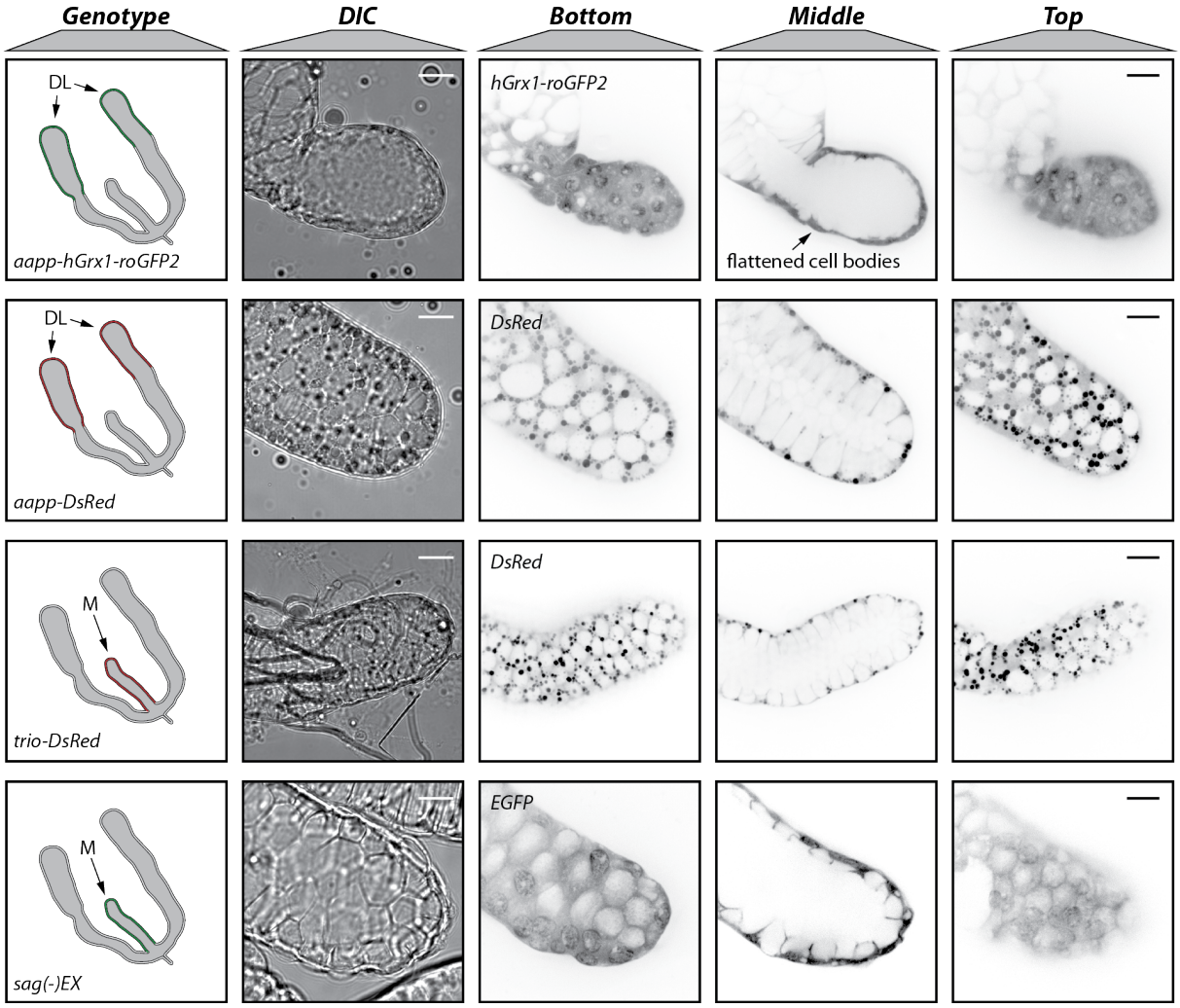

Figure 4. Different subcellular localizations of the expressed DsRed, EGFP and hGrx1-roGFP2 fluorescent reporters.

Differential interference contrast (DIC) and confocal fluorescence images of the distal-lateral lobes (*aapp-DsRed*, *trio-DsRed*) or the median (*trio-DsRed*, *sag(-)EX*) salivary gland lobes. Different z-sections (top, middle and bottom) of the same glands are displayed in the relevant fluorescence channel. Cell bodies of acinar cells in the tips of distal lobes expressing high levels of hGrx1-roGFP2 appeared flattened (as indicated) compared to cells expressing *aapp-DsRed*. Note that DIC and fluorescence images were taken with a Hamamatsu Orca Flash 4.0 V1 and a Yokogawa CSU X-1 camera, respectively. Images between different channels are therefore not completely matching although depicting the same salivary gland. Illustrations on the left depict the genotype of the lines and corresponding expression patterns. All images were acquired in the same microscopy session. Scale bars: 20 µm.

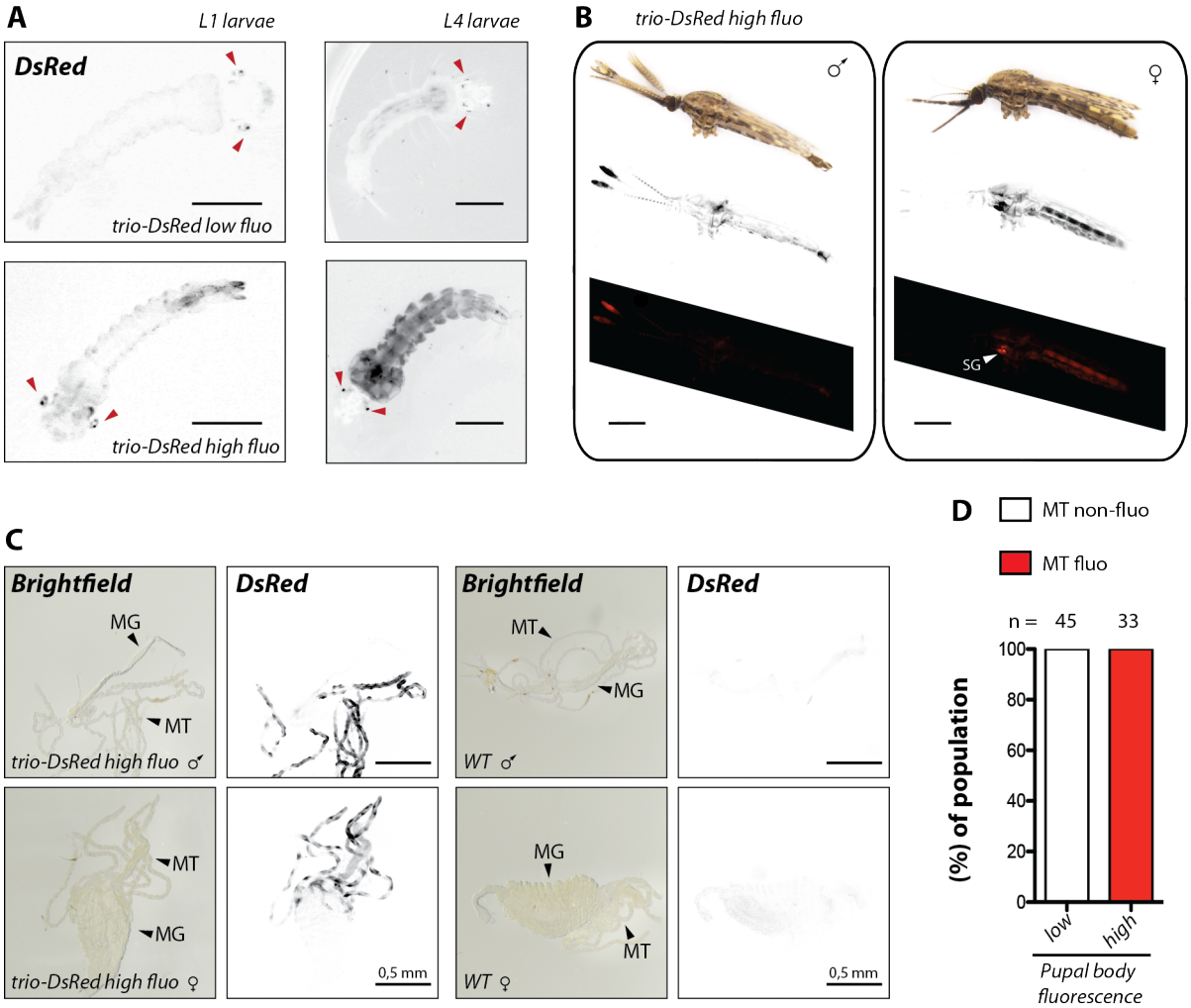

Figure 5. *DsRed* expression in Malphigian tubules (MT) of *trio-DsRed* mosquitoes is linked to ubiquitous *DsRed* expression in larvae, pupae and adults.
A) *Trio-DsRed* L1 and L4 larvae were classified as *trio-DsRed low fluo* or *trio-DsRed high fluo* according to their body DsRed fluorescence intensity. Red arrowheads point towards the DsRed positive eyes observed in the majority of larvae. Scale bar L1: 250 µm. Scale bar L4: 0.5 mm. **B)** Whole body fluorescence of *trio-DsRed high fluo* male and female mosquitoes. From top to bottom: brightfield, inverted DsRed fluorescence signal displayed in black and white and in red on black. Note that images were stitched from two separate images showing either the head or the abdominal part. Scale bar: 0.5 mm. **C)** Representative images of male and female midguts dissected from mosquitoes that displayed high body fluorescence at the pupal stage in comparison to *wild type* (WT: *G3*). Malphigian tubules (MT) and midguts (MG). Scale bar: 0.5 mm. **D)** Correlation of high body fluorescence at the pupal stage with *DsRed* expression in malphigian tubules (MT). Data were collected from two different mosquito generations. The number of analyzed mosquitoes is indicated above each column.

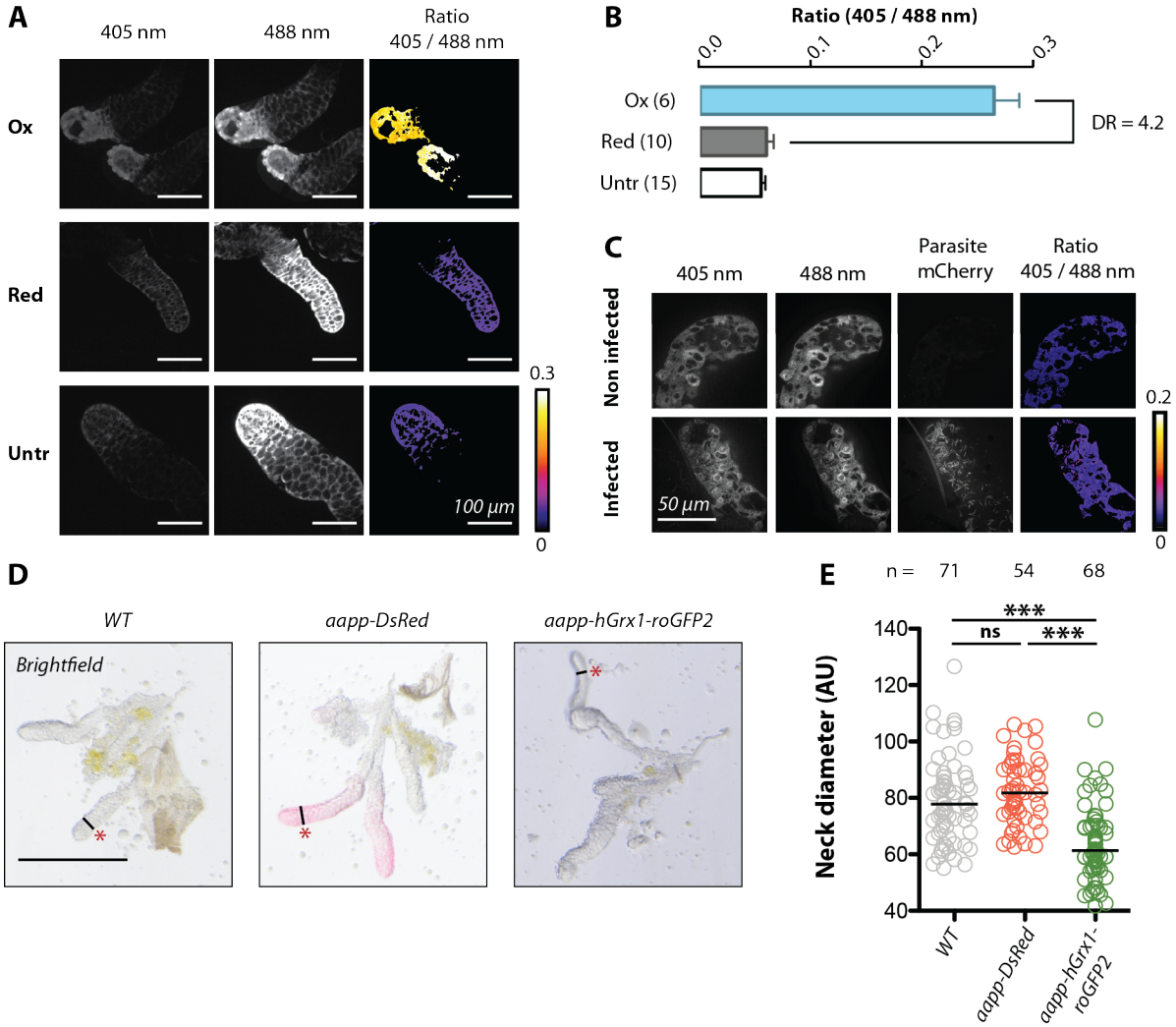

Figure 6. hGrx1-roGFP2 expressed in the salivary glands is functional but affects gland morphology.

A) Dissected salivary glands expressing *hGrx1-roGFP2* were incubated in diamide (ox), dithiothreiol (red) or N-ethylmaleimide (untr) and imaged at 405 nm and 488 nm wavelengths. The 405/488 ratio is given in false colors to indicate the oxidation level of the glutathione pool. Scale bars: 100 µm. **B)** Quantification of glutathione oxidation based on the 405/488 ratio. Salivary glands were treated as in (A). Numbers in parentheses indicate the number of examined salivary glands. DR: dynamic range. **C)** Image of a salivary gland infected with *mCherry*-expressing *P. berghei* sporozoites. Scale bar: 50 µm. **D)** Brightfield images of salivary glands from wild type (*G3*), *aapp-DsRed* and *aapp-hGrx1-roGFP2* females. The „neck region" of the distal-lateral lobes is indicated by a red asterisk and the measured diameter by a black line. Between 54 and 71 images were acquired for each line in ≥3 independent preparation and imaging sessions. Representative images presented here were all acquired in the same session. Scale bars: 250 µm. **E)** Diameter measurements of the distal-lateral lobe neck region of *aapp-DsRed* and *aapp-hGrx1-roGFP2* in comparison to wild type (*G3*). The number of measurements is indicated above each genotype. Note that only the diameter of one distal-lateral lobe per gland was measured. Data represent ≥3 independent experiments. The black line indicates the median. ***$p<0.0001$, one-way-ANOVA (Bonferroni's Multiple Comparison Test). ns: not significant.

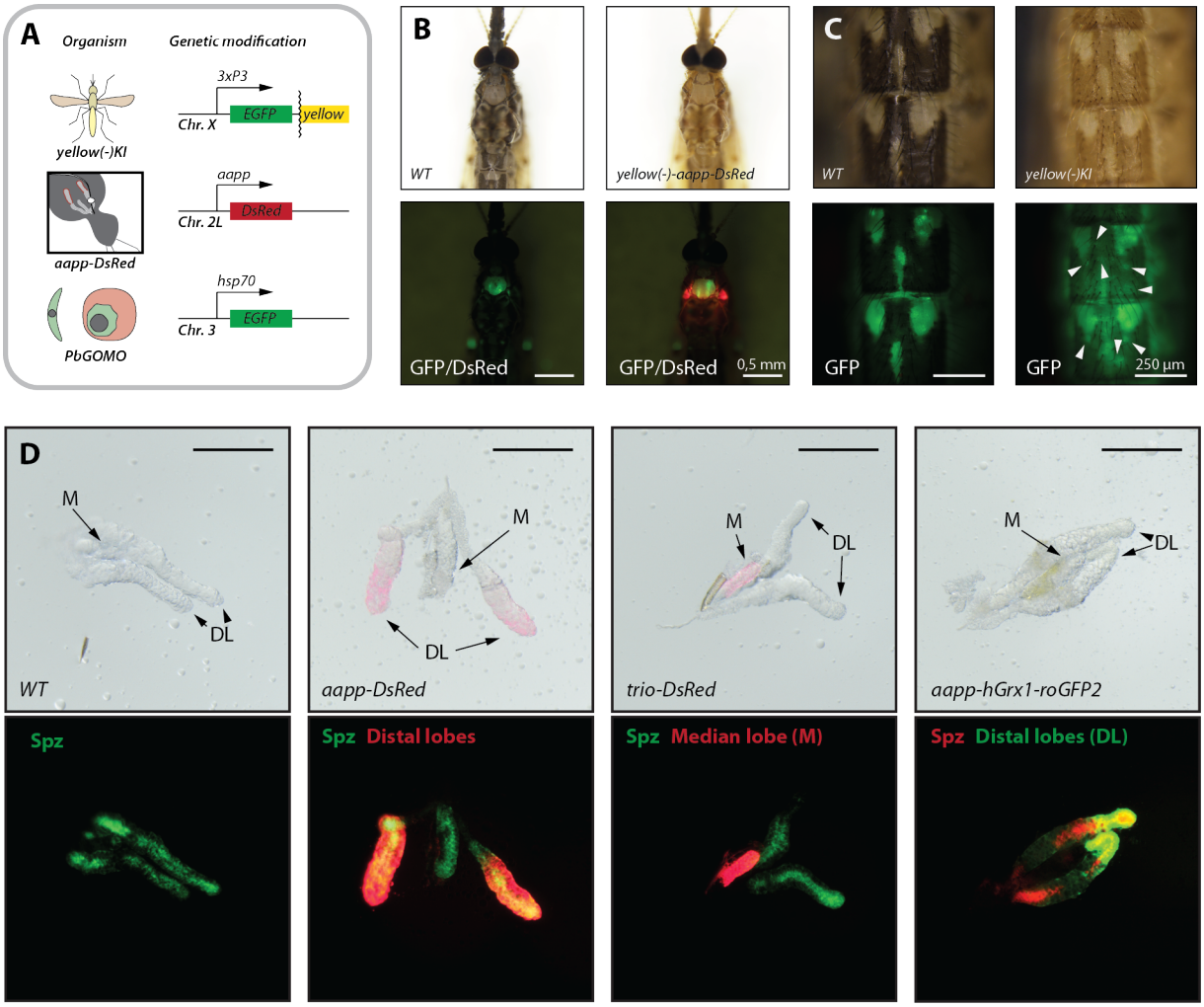

Figure 7. *Yellow(-)* and salivary gland reporter lines as tools for *in vivo* imaging. **A)** Genetic models used for *in vivo* imaging. Mosquitoes carrying the *aapp-DsRed* transgene were crossed with *yellow(-)KI* mosquitoes displaying reduced black pigmentation. Infections were carried out using the highly fluorescent *P. berghei* line *Δp230p-GFP* constitutively expressing *EGFP*. **B)** Pigmentation phenotype and salivary gland-specific *DsRed* expression in *P. berghei* infected *yellow(-);aapp-DsRed* and wild type (*WT*) mosquitoes. *GFP*-expressing sporozoites are displayed in green. Brightfield and DsRed signal of the same field of view. Scale bar: 0.5 mm. **C**) Images of the abdomen of infected *yellow(-)KI* and wild type (*Ngousso*) mosquitoes. Brightfield and GFP expression of the same field of view. White arrows point towards oocysts visible through strongly pigmented areas of the cuticle of *yellow(-)KI* mosquitoes. Scale bar: 250 µm. **D)** Images of salivary glands highly infected with *P. berghei*. Wild type (*WT*), *aapp-DsRed* and *trio-DsRed* have been infected with *GFP* expressing *P. berghei* (*Δp230p-GFP*) while *aapp-hGrx1-roGFP2* mosquitoes were infected with *mCherry* expressing *P. berghei* (*Δp230p-mCherry*). M = median lobe; DL = distal lobes. Scale bar: 250 µm.

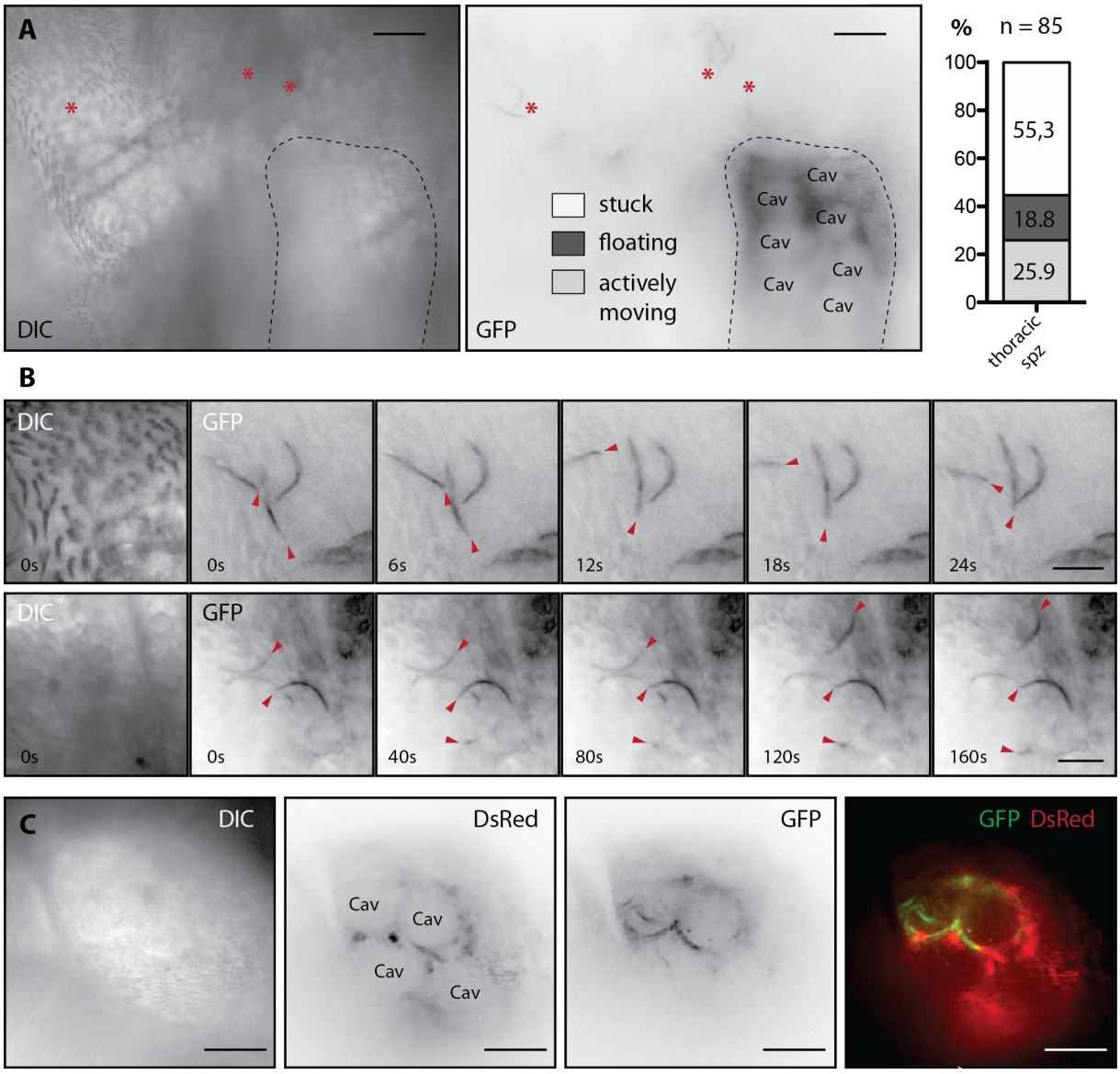

Figure 8. Confocal imaging of sporozoite motility in live mosquitoes.
A) View of the thorax area of a *yellow(-)-aapp-DsRed* female mosquito with persistent sporozoites indicated by red asterisks in the proximity of the salivary gland (outlined with a dashed line). Differential interference contrast image (DIC, left) and GFP signal (right). Note that *DsRed* expression in the salivary glands was strong enough to be visible in the GFP channel. Cav: salivary gland cavity. Scale bar: 20 µm. The behavior of observed persistent sporozoites was classified as "stuck", "floating" and "actively moving". The number of examined sporozoites is indicated above the column. Combined results of four different experiments. **B)** Time series of sporozoites showing active movements. DIC images at 0 s and time series of the GFP signal with 6 s (top) and 40 s (bottom) between frames. Red arrows point towards sporozoites displaying active movement. Scale bar: 10 µm. **C)** Sporozoites inside the salivary gland imaged through the cuticle of a living mosquito. Left to right: DIC, inverted signals of DsRed and EGFP in black on white and merge of both in colors. Note that the sporozoites follow the circular shape of the cavities. Scale bar: 20 µm.

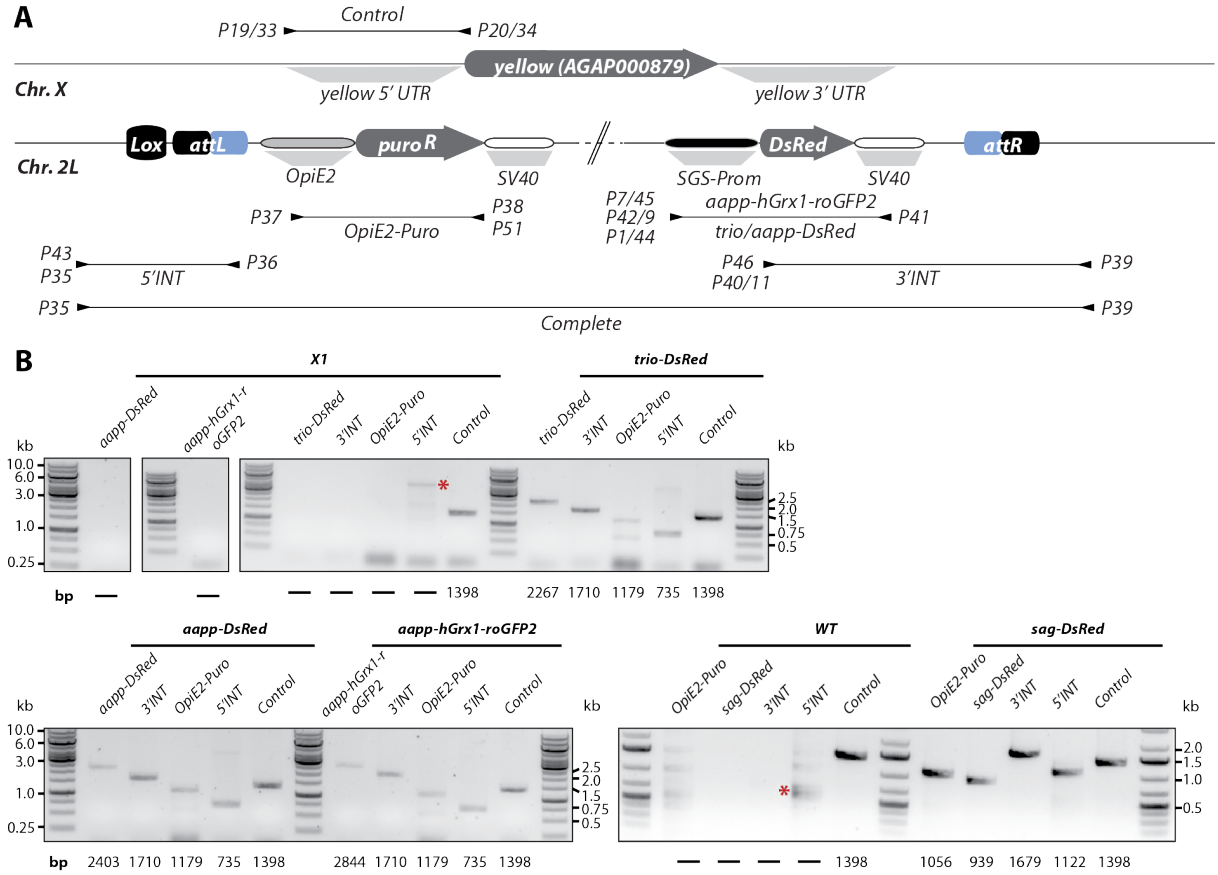

Figure 1 – figure supplement 1. Genotyping of the salivary gland reporter lines *aapp-DsRed*, *aapp-hGrx1-roGFP2*, *trio-DsRed* and *sag-DsRed*.
A) Schematic representation of salivary gland reporter transgenesis cassettes inserted on chromosome 2L. Fusion of *attB* and *attP* sites generate *attL* and *attR* sites after integration. The *Lox* site upstream of the transgene is a remnant of the fluorescence cassette initially required to select the docking line X1. Note that the illustration is not drawn to scale. **B)** Genotyping of generated transgenic mosquito colonies in comparison to *wild type* (WT: *G3*) or the parental line X1. Five different analytical PCRs were performed. The 5'INT and 3'INT PCRs amplify the integration borders upstream and downstream of the transgene, respectively. The presence of the puromycin resistance cassette was tested (OpiE2-Puro PCR). To ensure integration of the relevant fluorescence cassette, the PCRs aapp-DsRed, aapp-hGrx1-roGFP2, trio-DsRed and sag-DsRed were performed. In addition, a PCR control amplifying the 5'UTR of the *yellow* gene on chromosome X was included. Genotyping primers and amplified sequences are indicated with arrowheads and thin black lines, respectively, in scheme (A). Expected amplicon sizes are indicated under the gel images, (-) indicates that no amplification is expected. Red asterisks mark unspecific amplicons.

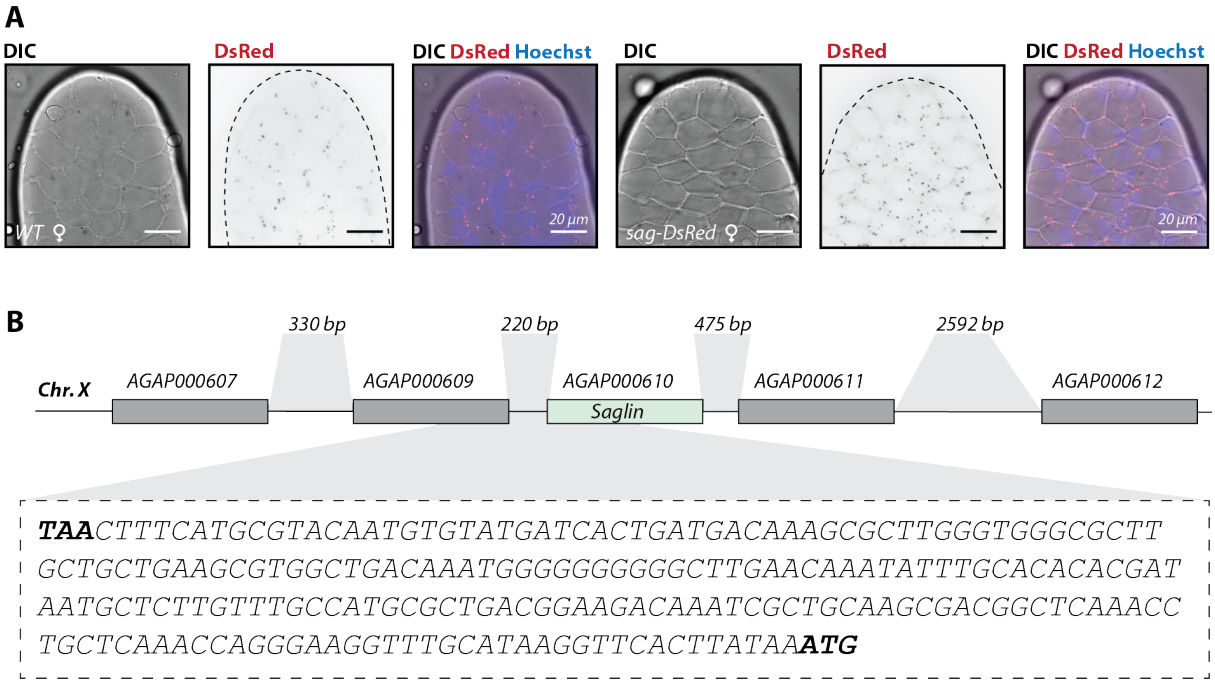

Figure 1 – figure supplement 2. The intergenic sequence between AGAP000609 and AGAP000610 (*saglin*) displays no promoter activity.

A) Images of the apex of the salivary gland median lobe from a *sag-DsRed* and a wild type female (*Ngousso*). Dissected glands were stained with Hoechst 33342 to detect the nuclei of acinar cells. The dotted black line in DsRed images indicates the outline of the salivary gland lobe observed in DIC. Scale bar: 20 µm. **B)** Genomic context of *saglin* (AGAP000610) with neighboring genes. The length of intergenic sequences is indicated above the scheme and the sequence tested for promoter activity located between AGAP000609 and *saglin* is shown. The stop codon TAA of AGAP000609 and the start codon of *saglin* are highlighted in black. The length of the cloned sequenced intergenic sequence was 220 bp (without stop codon of AGAP000609 and start codon of *saglin*). Note that the illustration is not drawn to scale.

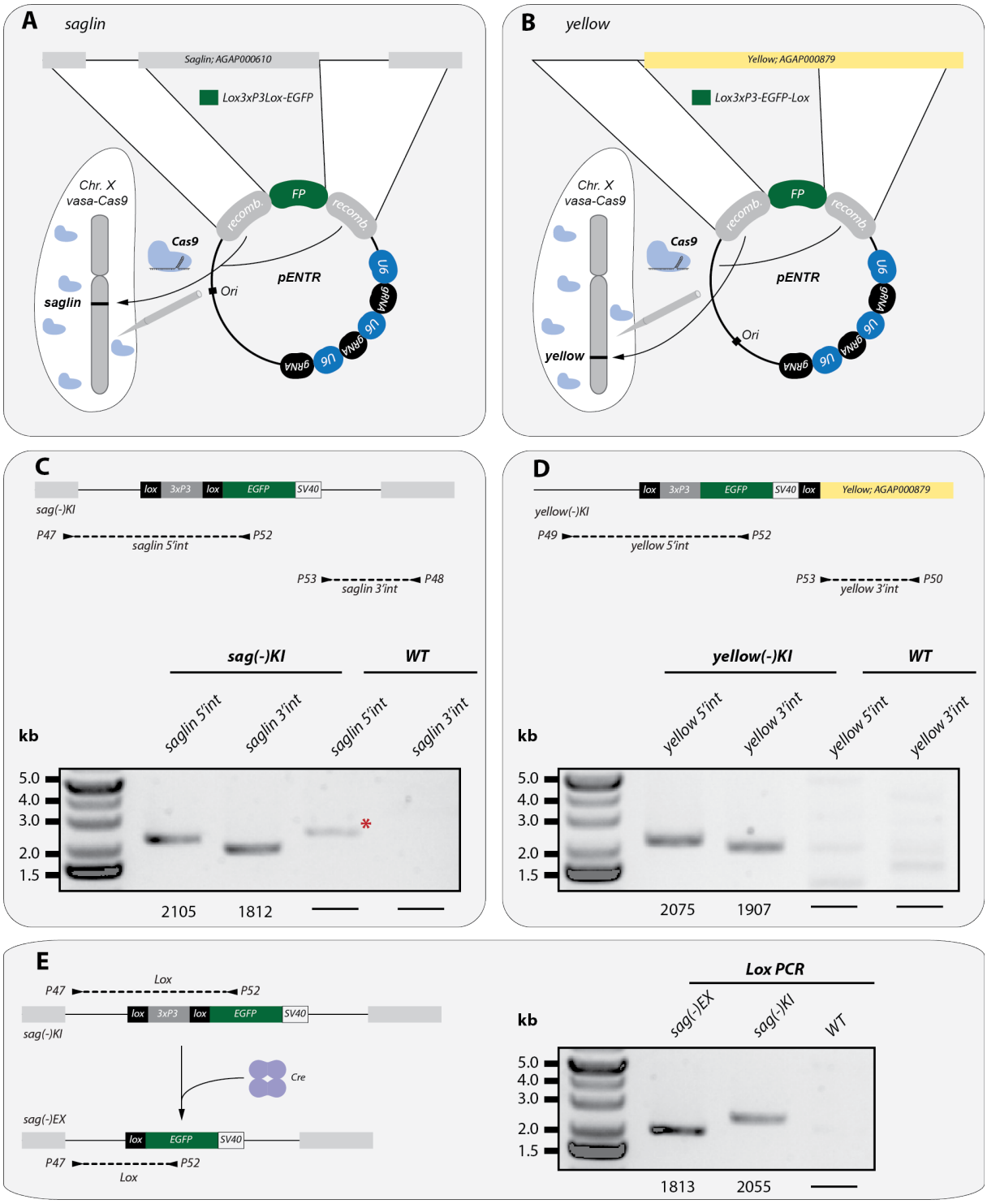

Figure 1 – figure supplement 3. Genotyping of *sag(-)KI*, *sag(-)EX* and *yellow(-)KI* mosquitoes.

Sag(-)KI (**A**) and *yellow(-)KI* (**B**) mosquitoes were generated by injecting embryos expressing Cas9 (*vasa-Cas9*) with plasmids carrying repair templates that contain a Lox3xP3Lox-EGFP or a Lox3xP3-EGFP-Lox cassette flanked with upstream and downstream sequences of the respective targeted loci, in combination with three guide RNAs specific for the *saglin* (AGAP000610) or *yellow* gene (AGAP000879). Genotyping of the 5' and 3' integration borders revealed successful integration of the transgenes into *saglin* (**C**) and *yellow* (**D**). The red asterisk marks an unspecific PCR product observed in the wild type control (WT:

1157 *Ngousso*). **E)** To investigate the native expression of the *saglin* promoter, the *3xP3* promoter
1158 initially used to select transgenic *sag(-)KI* mosquito larvae was removed by Cre-mediated
1159 excision. The loss of the *3xP3Lox* sequence in *sag(-)EX* mosquitoes was confirmed by PCR.
1160 Expected amplicon sizes are indicated under the gel images, (-) indicates that no amplification
1161 is expected (C, D, E).
1162

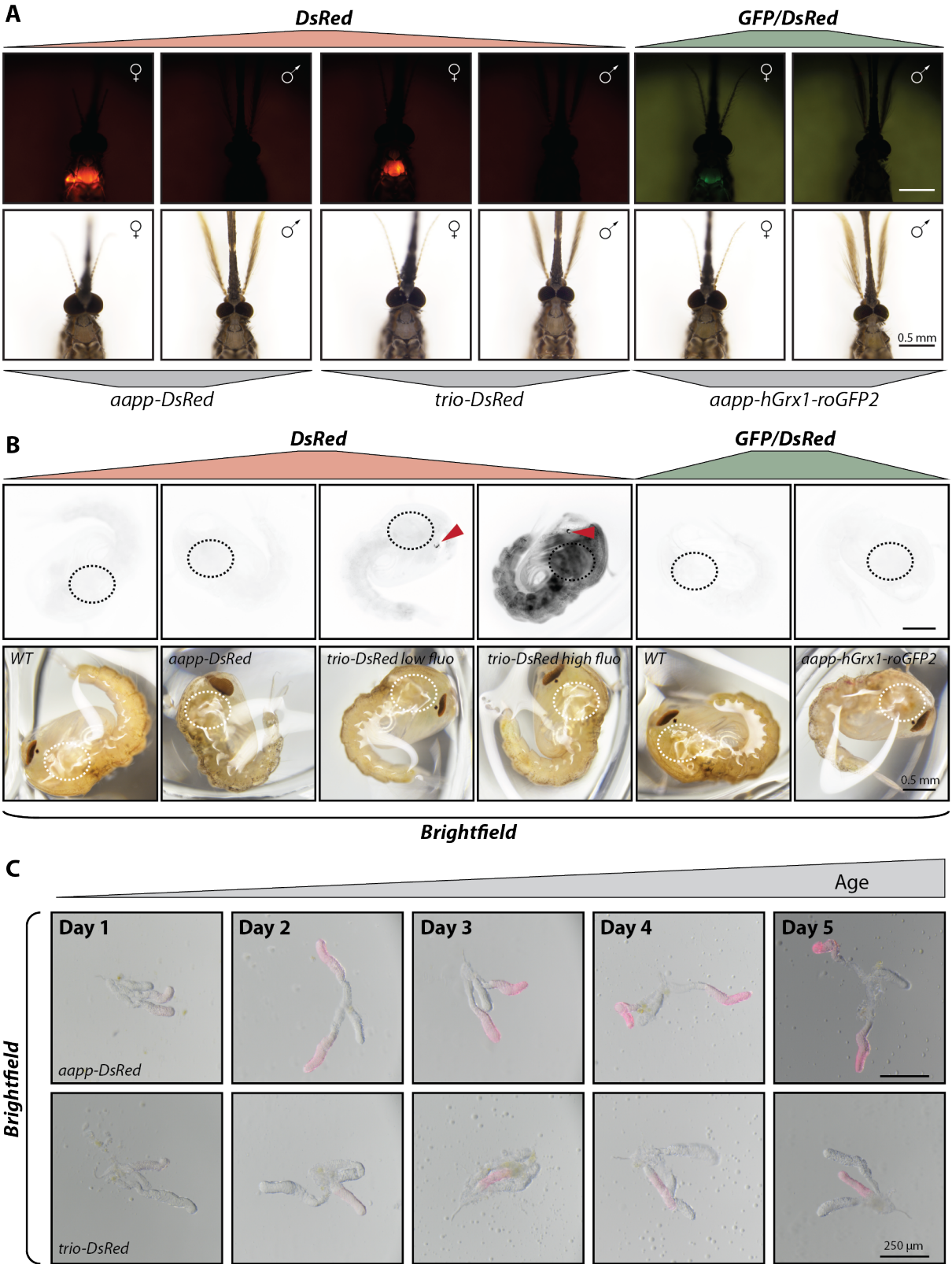

Figure 2 – figure supplement 1. Expression driven by *trio* and *aapp* promoters is female- and adult-specific and the fluorescent reporter accumulates after the emergence of adults.

A) Fluorescence and brightfield images of female / male pairs of *trio-DsRed*, *aapp-DsRed* and *aapp-hGrx1-roGFP2* mosquitoes. Note that all depicted mosquitoes were bred in synchrony and were seven day old (+/- 1 day). Scale bar: 0.5 mm. **B)** Fluorescence and

1171 brightfield images of *aapp-DsRed*, *trio-DsRed* and *aapp-hGrx1-roGFP2* pupae in comparison
1172 to *wild type* (*G3*). Dotted circles indicate the putative position of the salivary glands. *Trio-*
1173 *DsRed* pupae with low and high DsRed body fluorescence are shown for comparison. The red
1174 arrows indicate DsRed positive ocelli observed in most *trio-DsRed* pupae. Note that the
1175 fluorescence and brightfield images do not fully overlap as images pupae were able to move
1176 between the two pictures. Scale bar: 0.5 mm. **C)** Brightfield images of *aapp-DsRed* and *trio-*
1177 *DsRed* female salivary glands from day 1 to day 5 after hatching (a single image per day and
1178 per line). All images were acquired using the same settings. Scale bar: 250 µm.
1179

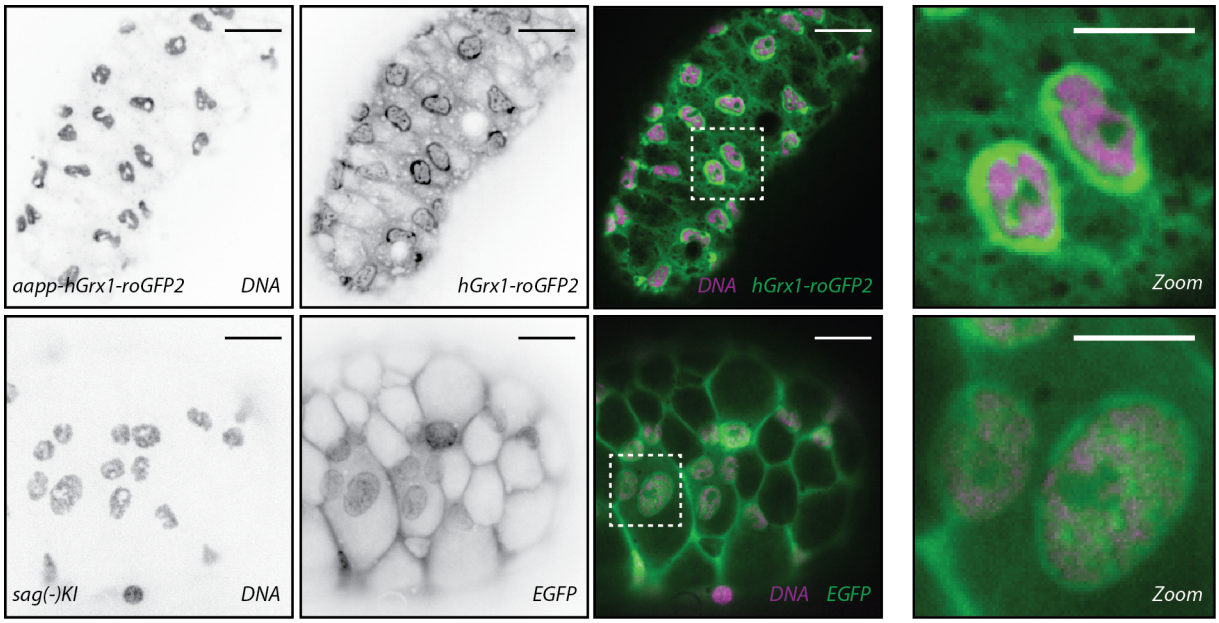

Figure 4 - figure supplement 1. EGFP and hGrx1-roGFP2 concentrate around nuclei of acinar cells.

Dissected salivary glands from *aapp-hGrx1-roGFP2* and *sag(-)KI* were stained with Hoechst 33342 (DNA) and imaged by confocal microscopy. The *sag(-)KI* line was chosen instead of the *sag(-)EX* line as it displays the same EGFP pattern but with stronger signal. Distal-lateral (top) and median (bottom) lobes are shown for *aapp-hGrx1-roGFP2* and *sag(-)KI*, respectively. Left to right: DNA and EGFP signals in black on white, combination of both signals in colors, and zooms of cells framed in the previous images. Scale bars: 20 µm except for zooms (10 µm).

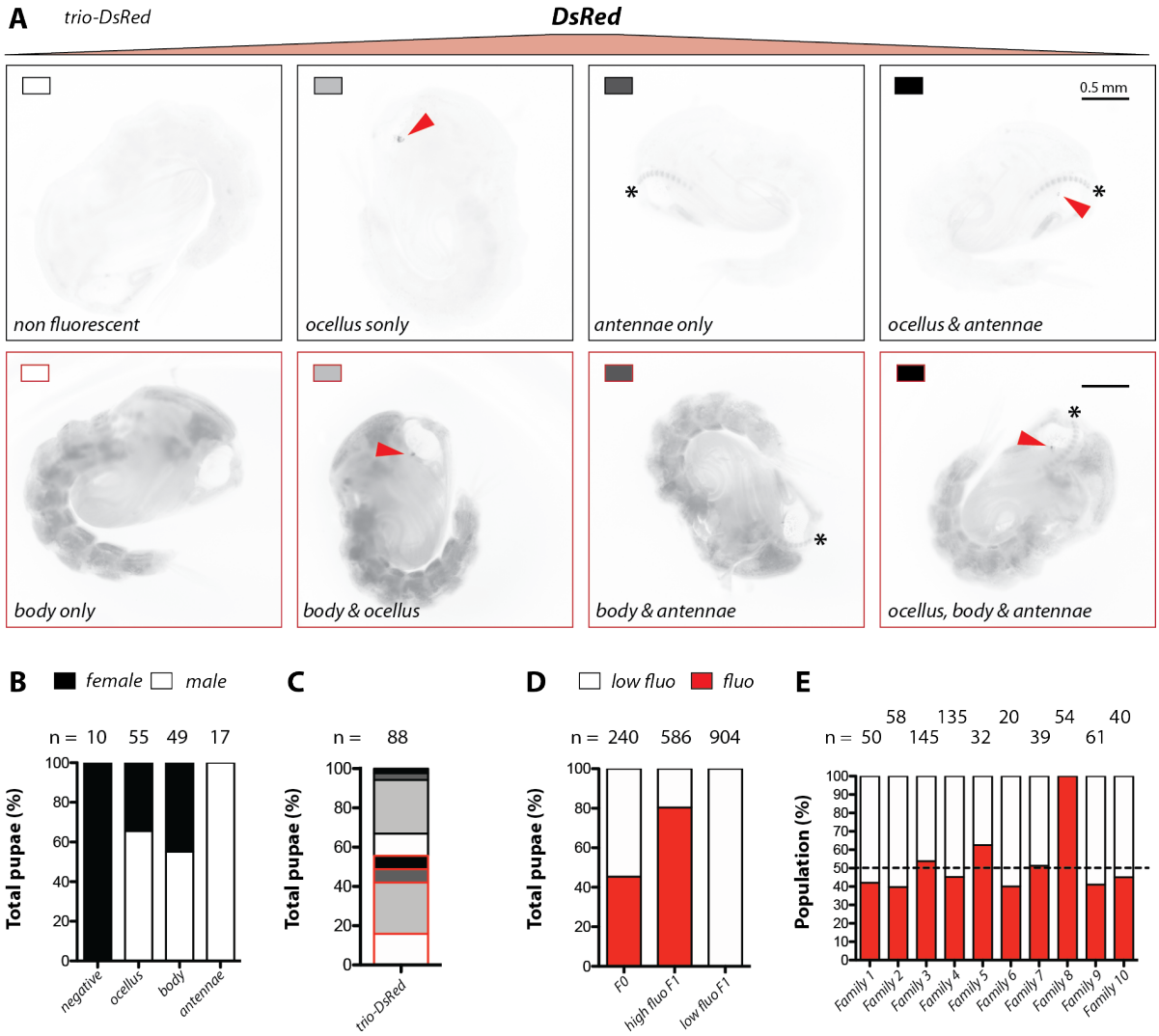

Figure 5 – figure supplement 1. *Trio-DsRed* pupae display high variability in *DsRed* expression.

A) Representative images of *DsRed* expression patterns in *trio-DsRed* pupae. A subpopulation of pupae displayed high body DsRed fluorescence (images in red frames) while remaining pupae showed no DsRed body fluorescence (black frames). Some pupae displayed fluorescent ocelli and/or fluorescent antennae. The presence of DsRed expression in body, ocelli and antennae occurred in different combinations that are represented by rectangles with different shades and frames. Scale bar: 0.5 mm **B)** Fluorescence patterns in pupae in relation to their sex. Number of pupae indicated above columns. Data pooled from four generations (≥20 pupae per generation). **C)** Proportion of each fluorescence pattern in relation to the whole population. Shading and framing of the different patterns as in (A). **D)** Proportion of pupae with high and low body fluorescence in the *trio-DsRed* colony (F0) and after intercrossing individuals displaying high or low pupal body fluorescence (F1). The number of analyzed individuals is given above each column. **E)** Females hatched from pupae with high body fluorescence analyzed in (D, high fluo F1) were kept separately and crossed to wild type males (*Ngousso*). The progeny of single females was evaluated at the pupal stage for body fluorescence (same color code as D, dashed line indicates 50% of the population).

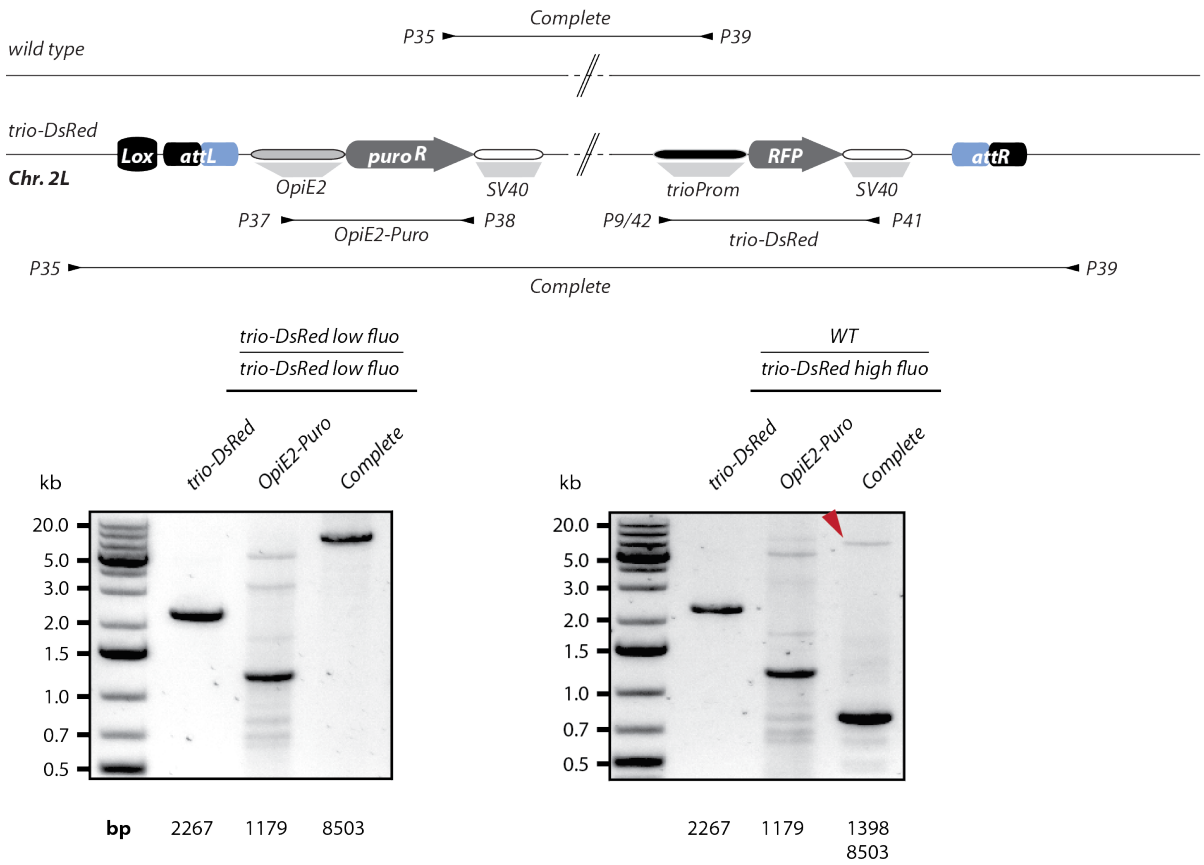

Figure 5 – figure supplement 2. Genotyping of *trio-DsRed low fluo* and *trio-DsRed high fluo* mosquitoes.

Genotyping of a female mosquito homozygous for the *trio-DsRed* low fluorescence transgene (*trio-DsRed low fluo*) taken from the colony generated by the intercross of pupae displaying no body fluorescence (see **Fig. 4 – Supplement 1D**) and of a female mosquito heterozygous for the *trio-DsRed* high fluorescence transgene (*trio-DsRed low fluo*) and the wild type allele (*WT*) obtained from family 1 (**Fig. 4 – Supplement 1E**). An illustration of the modified X1 locus containing the *trio-DsRed* transgene in comparison to the unmodified wild type allele is shown on top. Genotyping primers and expected products are shown as black arrows and lines, respectively. The length of the expected PCR products is indicated below the gel images. Note that for the heterozygous female carrying the *trio-DsRed* high fluorescence transgene, the smaller PCR fragment amplifying the unmodified locus dominates while the long PCR fragment representing the transgene containing allele is visible as a faint band at the upper edge (marked by a red arrow). The OpiE2-Puro PCR to verify the presence of the transgene gave several unspecific bands. PCRs were performed on genomic DNA obtained from single mosquitoes.

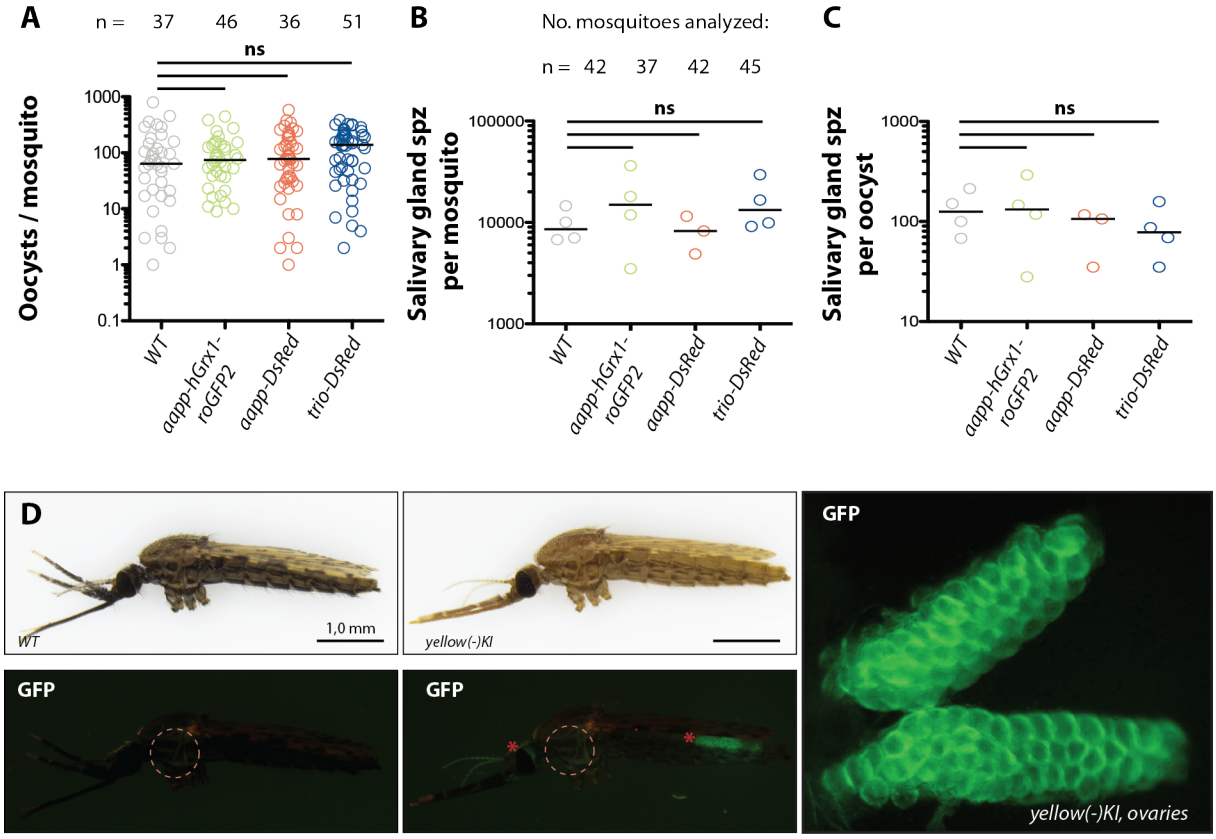

Figure 7 – figure supplement 1. Evaluation of *P. berghei* parasite infection in salivary gland reporter lines and background fluorescence in *yellow(-)KI* mosquitoes.
Oocyst (**A**) and salivary gland sporozoite (spz) (**B**) counts in infected *aapp-DsRed*, *aapp-hGrx1-roGFP2* and *trio-DsRed* females in comparison to *wild type* (*G3*) females. Data pooled from 3-4 experiments generated with three different mosquito generations. The total number of dissected mosquitoes is given above each genotype. Data points represent parasites counted per midgut (A) and mean number of sporozoites per mosquito in independent experiments (B). **C)** Number of salivary gland sporozoites (spz) per oocyst for all three reporter lines in comparison to *wild type* (WT: *G3*). The invasion rate was calculated using the data shown in (A) and (B). Each dot represents the mean of a independent experiments, the median is indicated by a bar. All data were tested for significance using a one-way-ANOVA (Kruskal-Wallis test). ns: not significant (p>0.05). **D)** GFP background fluorescence of *yellow(-)KI* in comparison to a wild-type (*Ngousso*) female. Combinatorial transcriptional activity guided by the *3xP3* and the endogenous *yellow* promoter drive EGFP expression in the eye and the ovaries of *yellow(-)KI* females (indicated by red asterisks). No EGFP-like fluorescence was observed in the throat region where the salivary glands localize (indicated by dashed red circle). Scale bar: 1 mm. The image on the right shows EGFP fluorescence from a dissected ovary of a *yellow(-)KI* female at higher magnification.

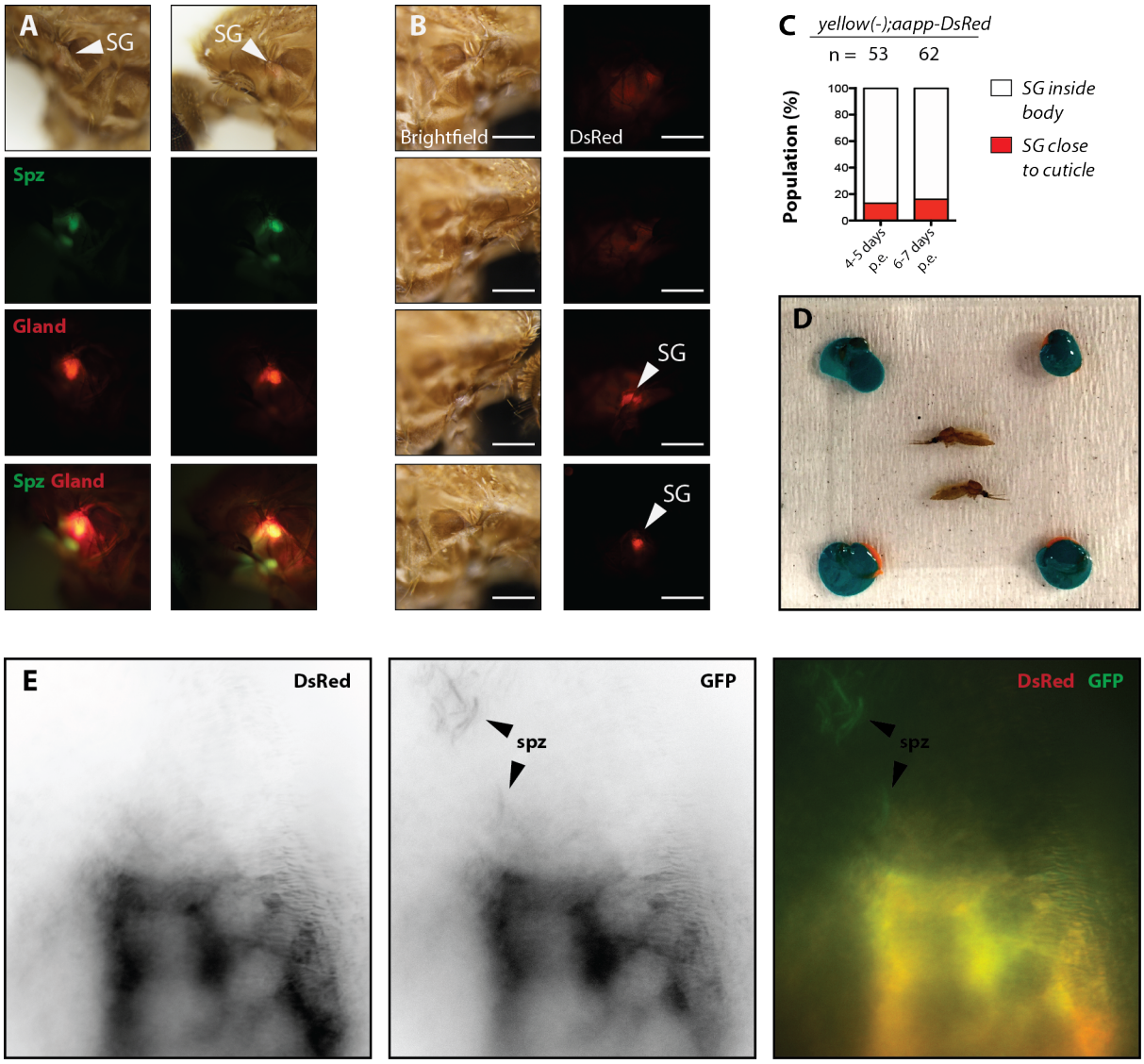

Figure 7 – figure supplement 2. Selection and sample preparation of mosquitoes for *in vivo* imaging and comparison of sporozoite and salivary gland fluorescence signals. **A)** Images of two infected mosquitoes with sporozoites (Spz, GFP channel) inside or close to *DsRed*-expressing salivary glands (SG, red channel). The bottom image was acquired with a filter set visualizing signals of DsRed and GFP. Salivary glands in both mosquitoes localised close to the cuticle. Their position is even visible in brightfield as a light red dot. **B)** The position of salivary glands varies between mosquitoes, either deep (rows 1 & 2) or close to the cuticle (rows 3 & 4). Brightfield (left) and DsRed (right) images of the same field of view. Images were acquired with the same settings. Scale bar: 250 µm. **C)** Quantification of salivary gland positioning according to the fluorescence pattern shown in (B). Two mosquito batches were evaluated per time point post emergence (p.e.). The number of evaluated mosquitoes is indicated above each column. **D)** Sample preparation before imaging. Legless mosquitoes were glued on a microscopy slide and covered with a cover slip underlaid with orange plasticine to avoid squeezing. Corner areas were subsequently coated with teal-colored nail polish to prevent the cover slip from moving. **E)** DsRed, GFP and merging the two signals of the image shown in Fig. 8A. Note that a significant portion of the DsRed signal is also visible in the GFP channel, whereas the sporozoites are exclusively visible in the GFP channel, potentially indicating spillover of the red signal due to the high DsRed concentration.

Movie 1. Sporozoites display active motility inside the mosquito.
Movie showing three sporozoites imaged in close proximity to the salivary gland. Sporozoites appear to be attached to a larger vessel and observed movements might be a combination of active motility and passive hemolymph flow. Imaging performed with a Hamamatsu Orca Flash 4.0 V1 camera using a 63x (NA 1.4) objective. GFP signal of a 3 min movie with 3 seconds between frames.

Movie 2. Sporozoites form accumulations close to the salivary gland.
Movie showing several sporozoites directly below the cuticle. Three sporozoites display different patterns of active movement. Imaging performed with a Hamamatsu Orca Flash 4.0 V1 camera using a 63x (NA 1.4) objective. GFP signal of a 2 min and 30 s movie with 2 seconds between frames.

Appendix 1 - figure 1.

Promoter sequences of the *trio*, *saglin* and *aapp* genes used to generate the mosquito lines *aapp-DsRed*, *aapp-hGrx1-roGFP2*, *trio-DsRed* and *sag-DsRed*. Nucleotides highlighted in red are part of the primer sequence used to amplify the promoter sequence. Sequences with a grey background indicate the 5'UTRs of the *trio* and *aapp* transcript, respectively.

***aapp* promoter sequence (AGAP009974, 1673 bp):**

CTTTTCTTTTACCCTTTGTAACACGCTAATAACGAAAGACCTCCTGCGTGTTAGTACG
TGGTGAGGATGATGCGTTTTAGCCTAGCTAGTATTCAAAAAACCTATTAATGCAACAATTAC
AGTGTGAGGTTACAAAATGGAATTAATTAAACACACTGCTCAACACAGCCATCGTGCTGCAT
CGTGCTTTGTTGAGGCGCAACAGTTAAATTGTAAGTGCAACCACCGGTATAGAGAGCTGCTT
TTGGCAAATGATATGGAATTGTGCTAAATTATGTAATGTTTTTTTTAACTAACTCGTTTACC
CGTTAATGGTGGAATGTTTGCAGGTGCGTAGATTAATTTTTTTTAAATGTGCAAATGGAGAA
AACAGGATAACGCAAAAGTATTTCCTTCGCTGTAGTAATAGGCTATTATTTATGTACGTCTT
TATGTGACCCCGCTAGTGTTGGCTGTATTTTATATCTGTAGGTAAATGACGCGCTATGTATT
GTAATAAAATTGGACAAACATTTGCATGTACGATCTGTTAGCTTAGAGAATAAGTATTTTTC
TTTTTCGCTACATTTCTCTAAATTCGACCGACGATGACTGTTTTAGGTGTTTTTTCGTAACT
TGATCAAGGTAACACCTTTTCTTGGCGTAACGTCCTACGCGGACATGCCGGCCGGCCTTATT
CAGGCTTTCGAGACTTAATTCATTACCACGTAGCCGGATAAGTCCAATCCTTGCACAACGGG
GGAACGGGTGTCCATTTCAGGCTTGGGCCCATGACGGGCATGTTATTGAGTCGTTCGAGTTG
ACGACTGTACCATGGGACCGCCCCATTTTTGGCAGTCCATTGATCGTTACGTCGTTTTACGT
CTACTGAAGGATGTCCGTTATCAGGTCAAGTCCAGCATAGATTAAGTCTCCCATACGAAGGA
TTGATTAGCTCGAGACTTAATGTTATATACAAAATTCTTATACATGTTCTAGATCAGGATTG
TTGCGCTACACTGTCTTCCATGTCGATCTTCTATATTCAGTTTTTGGCACAGTGATCGTCAC
TGTAATCTCAATAGATTTGAATTTCAATACTTCTATGGGAGGAGGATGAGTAGAAAGGTGTC
CAAAGCGCTGGATCTATGGCTGCAACTCCTCATGCTTGTAAGCACCCGACAGCCAATTCGAT
CTACCTGACCTGATGCGGTATTCGAACTAAAAGCACAGATCAAGCACTGTTTCACACGATCT
GAAGCACTGTTCTACTGCAAAGATAAGTGCATATTAGTTATTTTTCATACCGATCTTCACTG
CGACGGTTTAGCGATCTTCATTATTTTCCACCTTCACCCCTCAACCCAGGGAGTGCGCTTTT
CCCCGTCGAGATAAAATTACTAAATGTAAACTTTGCATGCAATTATGTAGCTGTATGGTAAG
CAAATAAAAATCTTTCCTCCTATTGCAACACGTCGCTTGTTTGCAGCGGATATTTGCCCACA
GTAAAGCCCGATCGCCTGTGCATTGTGTTTAACACGTGCTGCAAGCTGTATCAATACCGATC
GATTGTATGATTCCACGATCTTCGTGTGGTATAAAAACGGCGCTGAACAGCAGTAAAGATCA
TCACTTACATTTGTTTTATTCTCCACGGAGTCAGTGAAATAATACCACAACAACAAAAAAAC
G

***trio* promoter sequence (AGAP001374, 1537 bp):**

TTTTCTGAGGTGATCTTTCGAAAAGATCGATCGACCGACCCCCAACGGCAACTCTCCC
TCGGATGACCTCAGCCCAGAATAGGCATTCTTTCAGCAAGTCATTCTATCATCCCTTTTACA
TCTTACGTTACTCCAAAAAAAGAGAAGCTTTCCACCCCAAAGCTTTCGTTGTGGTGCAGCTT
TCGATGGTGATCGCGATCACGGTACCACACGTACGTTTGTTTGCTACTCTCGCTCACCGTTT
TCTTCGATTTCGTGTCTCGGGTACCGTTTGCTCGGTGCGGTAGTGCTGCGAAGAAAGCCGTT
GGCCGAGAGAATAATGCTCACTTCGGCTGCACGCAACTCGCCGTGCCACAGCCGTGGAAGGG
GTAGGTTGGATGGTCGGGGTCGGGACCGCAACGCCGAAGTGAACGCCGGCGTGCCAGCGAAC
GATCGCACCCCGGCACAGTCCAACTGCGTCGCTGGGCGCGCTCGGCGGACGGTTCTCGGTGT
GTGCGCCCCCTTTGGTGCTCATCCCTCATATCTCATCTCATCCTTTCGCGCTGCTCGCGGTT
CCCGCAGAACCACGCGCGAGAGGGAGTTGCGCGAACCAGGGAGAGCCCGACACCTGGGCAGC
GTCCAGGCGGACCTGTTCGGGAACGGTCGCGGTGTATAAAACTCGATTCCCGCCCGCCGTTA
GGTAACAGTCCATTGTGTAACGTTGCCGGGATCGCGAGCCATCCTGCAGGAACACAGCCGTG
CGAGTTTGTGTGCGCGTGTATTTTGCCTACAAGCAAGTGAGCAGCAATCAGTGAGAACAACA
TCTAAAACAGAAAAACAAACAGTGAACTACAGTGCTGTGGAGCAGTGGAAATTGGTGTTAAT
TGAAGAGCTTTGTACATCGATCACACGGACAACCACGCACGTGGAGAAAGTTCTGCTGCGGT
GCGGGTTACTTGCGTACACCACATTAAACATTGTGTGTGGCATTTAAAATAAATATACTCGC
GCCCTCCCCTCAGCTGCTCTCGCGGGCACGCCCGATGCCAGAGGTCGCCCCGACCGGACATT
GAACGTGGAAAGAAGAAAGTTGTCGGTTGTTTACACTTCCGTCCTGAGTGGTGTTGTGGCTA
CCGTTTGTGACCGTTGGTGAAATAAAGTAACATACCCCTCCCGAGGGCAGCAGCGACAATGA
CCTCCGGAAATTCGATAACAATACGTAAGTTACTTTCATTTTTTGCAAATTAAATTACCTCG
TGATAATTGAGTGGAGTGAGTAGGTACAGGTTGTTAACGCGTCTTTTGTTTAGTTCGGCAAT
CCGGATCCGAAGATGAGAGGAGATTGCCTCTGATGATGATGTTATCATGATTGCTTGTGTAA
CGACGCAAAGATTCTCAGAGAACAACTTCTCCCAACATAATTAATCTTGTTGAAGGGTCTGT
AAACACGTGGTGGGATATCTTACAACTGAACCAATATTCGACCGATAGTATAAAGTCCTTCG
CACCATCGATGCGTTTACCATTTTCCCATAAAATCAATCTGCTCCCAGTTACA

***sag* 5' upstream sequence without promoter activity (AGAP000610, 220 bp):**

CTTTCATGCGTACAATGTGTATGATCACTGATGACAAAGCGCTTGGGTGGGCGCTTGC
TGCTGAAGCGTGGCTGACAAATGGGGGGGGGGGGGCTTGAACAAATATTTGCACACACGAT
AATGCTCTTGTTTGCCATGCGCTGACGGAAGACAAATCGCTGCAAGCGACGGCTCAAACCTG
CTCAAACCAGGGAAGGTTTGCATAAGGTTCACTTATAA